iScience

CellPress
OPEN ACCESS

Article

Atrial natriuretic peptide signaling co-regulates lipid metabolism and ventricular conduction system gene expression in the embryonic heart

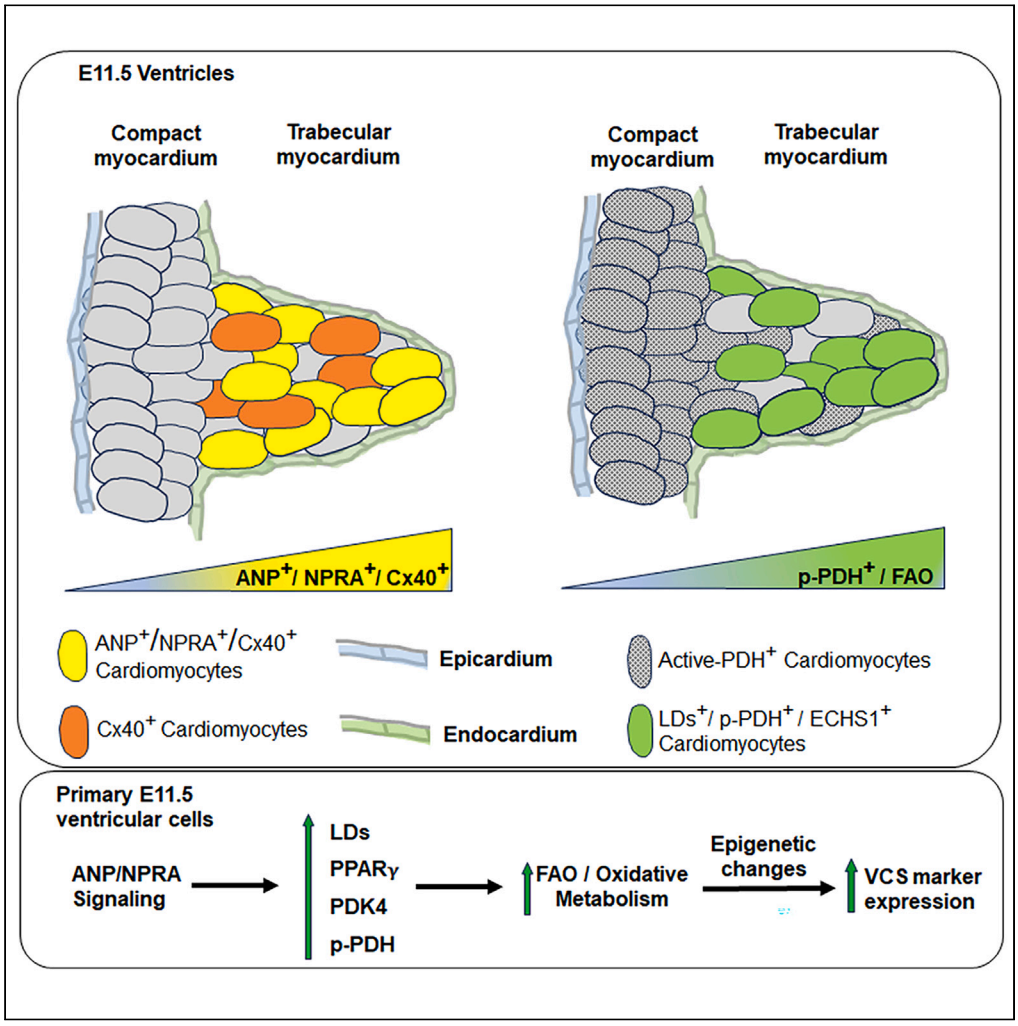

Abhishek Mishra, Mahtab Tavasoli, Stanislav Sokolenko, Christopher R. McMaster, Kishore B.S. Pasumarthi

Kishore.pasumarthi@dal.ca

Highlights

ANP/NPRA and markers of VCS and FAO are enriched in E11.5 trabecular myocardium

ANP stimulates VCS cell proliferation and marker expression in primary cell cultures

ANP regulates lipid storage, FAO and oxidative metabolism in E11.5 ventricular cells

Inhibition of PPARγ or FAO blocks stimulatory effects of ANP on VCS marker expression

Mishra et al., iScience 27, 108748
January 19, 2024
https://doi.org/10.1016/j.isci.2023.108748

iScience

CellPress
OPEN ACCESS

Article

Atrial natriuretic peptide signaling co-regulates lipid metabolism and ventricular conduction system gene expression in the embryonic heart

Abhishek Mishra,[1] Mahtab Tavasoli,[1] Stanislav Sokolenko,[2] Christopher R. McMaster,[1] and Kishore B.S. Pasumarthi[1,3,*]

SUMMARY

It has been shown that atrial natriuretic peptide (ANP) and its high affinity receptor (NPRA) are involved in the formation of ventricular conduction system (VCS). Inherited genetic variants in fatty acid oxidation (FAO) genes are known to cause conduction abnormalities in newborn children. Although the effect of ANP on energy metabolism in noncardiac cell types is well documented, the role of lipid metabolism in VCS cell differentiation via ANP/NPRA signaling is not known. In this study, histological sections and primary cultures obtained from E11.5 mouse ventricles were analyzed to determine the role of metabolic adaptations in VCS cell fate determination and maturation. Exogenous treatment of E11.5 ventricular cells with ANP revealed a significant increase in lipid droplet accumulation, FAO and higher expression of VCS marker Cx40. Using specific inhibitors, we further identified PPARγ and FAO as critical downstream regulators of ANP-mediated regulation of metabolism and VCS formation.

INTRODUCTION

The ventricular conduction system (VCS) is a downstream component of the cardiac conduction system and regulates the rhythmic contraction of ventricles. The VCS is composed of the bundle of His, bundle branches, and Purkinje fibers. Although common progenitors for VCS cells and working cardiomyocytes have been identified,[1,2] there is scant information on divergent mechanisms regulating these cell fates. Understanding mechanisms regulating VCS formation is critical for the repair and replacement of injured regions in VCS disorders resulting from genetic and acquired etiologies.[3,4] Recent studies uncovered critical roles of paracrine/autocrine factors such as neuregulin-1 (NRG-1), endothelin-1 (ET-1) and atrial natriuretic peptide (ANP) as well as various transcriptional factor networks in the VCS formation.[5–9] While the ability of NRG-1 to induce VCS specific reporter gene expression was restricted to E8.5 to E10.5 stages of mouse heart development,[7] ANP treatment was effective beyond E11.5 stage in increasing the expression of VCS markers such as connexin 40 (Cx40) and hyperpolarization-activated cyclic nucleotide-gated channel-4 (HCN4).[8] Additionally, genetic ablation of the high-affinity receptor for ANP (natriuretic peptide receptor-A/NPRA) revealed reductions in the expression of Cx40 and HCN4, and a hypoplastic Purkinje fiber phenotype.[8] Although the importance of the ANP/NPRA signaling cascade in VCS development is well established,[8] the underlying mechanisms are not fully characterized.

Expression pattern of ANP in the ventricular chambers from E8.5 to E15.5 coincides well with the VCS development.[10] Although ANP expression is downregulated in the trabecular myocardium (TM) by E15.5,[10] it persists in Purkinje fibers of the fetal and adult hearts.[11–13] Like ANP, Cx40 is also expressed throughout the ventricular trabeculae between E9.5 and E16.5 stages of heart development and it becomes progressively restricted to a well-organized VCS network after E16.5 stage.[1,6,14] While Cx40+ VCS cells were shown to exit cycle by E13.5 to E18.5,[15] cell cycle activity in the compact myocardium (CM) remains higher than that of TM throughout fetal heart development.[16] It was also shown that the VCS cell differentiation continues throughout fetal and early postnatal heart development.[1] Collectively, these studies indicate that ANP positive VCS cells continue to maintain Cx40 expression in the postnatal heart. However, mechanisms regulating VCS cell proliferation and differentiation are not very well characterized.

Myocardial cells show a shift in substrate utilization from glucose to fatty acids in postnatal hearts and also during cardiomyocyte differentiation in pluripotent stem cell cultures.[17] Several reports documented positive effects of exogenous fatty acids on cardiomyocyte maturation.[18] However, the role of lipid metabolism and signaling in the embryonic heart development and VCS cell differentiation has largely been overlooked. While variants in genes coding for regulators of fatty acid oxidation (FAO) were shown to cause conduction abnormalities in newborn children,[19] their effects on conduction system development are not known. Homozygous deletions of genes coding for carnitine

[1]Department of Pharmacology, Dalhousie University, Halifax, NS, Canada
[2]Department of Process Engineering and Applied Science, Dalhousie University, Halifax, NS, Canada
[3]Lead contact
*Correspondence: Kishore.pasumarthi@dal.ca
https://doi.org/10.1016/j.isci.2023.108748

palmitoyltransferase 1b (CPT1b: transports long chain fatty acids into mitochondria), short-chain enoyl coA hydratase (ECHS1: key enzyme in FAO) and members of peroxisome proliferator activated receptor (PPAR) family led to embryonic lethality in mice.[20–23] However, the effects of these genetic deletions on VCS development have not been studied.

ANP is known to regulate lipid mobilization and lipid metabolism in noncardiac cell types such as adipose tissue, liver and skeletal muscle.[24,25] ANP also promotes adipogenic differentiation of epicardial derived cells and increase adipose tissue accumulation in adult atria.[26] Lipid droplet accumulation is critical for neural progenitor cell proliferation and differentiation.[27] Despite these reports, potential links between ANP/NPRA signaling, lipid metabolism, and myocardial cell differentiation in the embryonic heart have not been investigated. Using histological sections of E11.5 mouse hearts, we show that ANP/NPRA-rich trabecular region reveals VCS marker expression (Cx40 and HCN4) in cells positive for lipid droplet accumulation. In addition, using E11.5 ventricular cell cultures, we show that ANP plays a key role in VCS cell proliferation and differentiation by promoting lipid droplet accumulation, mitochondrial oxidation and associated gene expression changes. Overall, this study underscores the importance of peroxisome proliferator activated receptor-γ (PPARγ) and mitochondrial FAO in VCS formation during heart development.

RESULTS

Embryonic day 11.5 heart reveals transmural gradients for expression of ANP/NPRA and markers of VCS cells and energy metabolism

Thin transverse sections (10μm) of E11.5 embryos were processed for immunostaining with antibodies specific for ANP, NPRA, and sarcomeric myosin heavy chain (Sarc. MHC) as well as VCS markers (Cx40 and HCN4) (Figures 1A–1F). The immunostained cells in the TM and the compact myocardium (CM) were counted from the left ventricles in all sections. The percentage of Sarc. MHC+ cells was significantly lower in the TM compared to the CM (70% in TM vs. 95% in CM) (Figure 1G). Further, immunolabelling with ANP and NPRA also revealed a differential expression pattern in TM vs. CM. The percentage of ANP+ cells was 8.4-fold higher in the TM (64% in TM vs. 7.6% in CM, Figure 1H) in agreement with earlier studies.[28,29] The percentage of NPRA+ cells was 12.6-fold higher in the TM compared to the CM (72.7% in TM vs. 12.8% in CM, Figure 1I). Consistent with ANP and NPRA staining patterns, the percentages of Cx40+ and HCN+ cells were also higher (4.4- and 3-fold respectively) in the TM compared to the CM (Figures 1J and 1K). Co-immunolabelling experiments with antibodies for ANP and Cx40 revealed many cell clusters in the TM co-expressing both markers (Figures 1L–1N). While there was a clear overlap between these two markers, Cx40 expression also appeared in the adjacent TM cells negative for ANP staining (Figure 1N). Examination of staining patterns in parallel sections indicated a clear overlap between NPRA and Cx40 expression in the primitive VCS forming trabecular zones (Figures 1O and 1P).

A switch in the energy metabolism from glucose to FAO plays a critical role in ventricular cell proliferation and differentiation during cardiac development.[17] Given the role of ANP in lipid storage and metabolism in adipose tissue,[26,30] we reasoned that the transmural ANP/NPRA signaling gradient in developing ventricles could be responsible for zonal differences in cellular metabolism thereby facilitating VCS cell differentiation in the TM. Phosphorylation of the enzyme pyruvate dehydrogenase (*p*-PDH) is known to inhibit its ability to convert glycolysis-derived pyruvate to Acetyl CoA,[31] whereas enoyl CoA hydratase (ECHS1) is an essential enzyme in the β-oxidation pathway of fatty acids.[32] The percentages of cells positive for *p*-PDH and ECHS1 were significantly higher in the TM compared to the CM (1.4-fold and 4.4-fold respectively, Figures 1Q–1T). Notably, both right ventricle (RV) and interventricular septum (IVS) also showed significant correlations between ANP/NPRA and markers of VCS cells and FAO (Data S1). Collectively, these results suggest that ANP/NPRA signaling could stimulate higher rates of fatty acid metabolism in TM ventricular cells and promote VCS marker gene expression.

Exogenous ANP treatment increases VCS marker protein levels and VCS cell proliferation in E11.5 ventricular cell cultures

To directly examine whether exogenous ANP can increase the protein levels of VCS markers, we treated E11.5 ventricular cell cultures with ANP (0.3 μM) and or an NPRA inhibitor (A71915, 1 μM) daily for 72 h. Protein lysates prepared from primary cultures treated with or without ANP and A71915 (A7) were subjected to western blotting and nitrocellulose membranes were probed with antibodies specific for Cx40, HCN4 and GAPDH (Figure 2A). The expression levels of Cx40 and HCN4 normalized to corresponding GAPDH levels were significantly higher (2.5- and 1.3-fold respectively) in ANP treated cultures compared to the controls (Figures 2B and 2C). There was no significant difference in the expression levels of VCS markers between control cultures and cultures co-treated with ANP and A7 (Figures 2B and 2C). Since many E11.5 embryos are required to perform western blotting experiments, in-cell westerns on cells grown in 96 well plates were also performed as an alternative method to examine the effects of ANP on VCS marker proteins. Marker protein signal in each well was quantified after immunostaining and normalized for the cell number using Hoechst nuclear staining. Consistent with the western blotting results, in-cell westerns also revealed a significant increase in Cx40 expression in ANP treated cell cultures compared to the control cultures (1.2-fold vs. control, Figure 2D). Co-treatment of primary cultures with A7 and ANP led to no significant change in Cx40 expression compared to the levels seen with control cultures (Figure 2D). Whereas expression levels of Sarc. MHC were not significantly altered in cultures treated with ANP and or A7 (Figure 2E).

Next, E11.5 ventricular cells treated with or without ANP and A7 for 24 h were analyzed for any changes in cell proliferation. Immunostaining with Cx40 and Sarc. MHC antibodies followed by click-iT EdU (a modified thymidine analogue) or pan-phospho-Aurora kinase (AURK) staining were performed to identify VCS cells undergoing DNA synthesis (Figure 2F) or cell division (Figure 2G) respectively. Cell counts performed in a blinded fashion revealed significantly higher DNA synthesis and proliferation rates in Cx40 expressing VCS cardiomyocytes (EdU+Cx40+Sarc. MHC+ and AURK+Cx40+Sarc. MHC+) in cultures treated with ANP compared to control cultures (~2.3-fold for EdU+Cx40+Sarc. MHC+ cells and 3.1-fold for AURK+Cx40+Sarc. MHC+ cells vs. control, Figures 2H and 2I). AURK staining in VCS cells

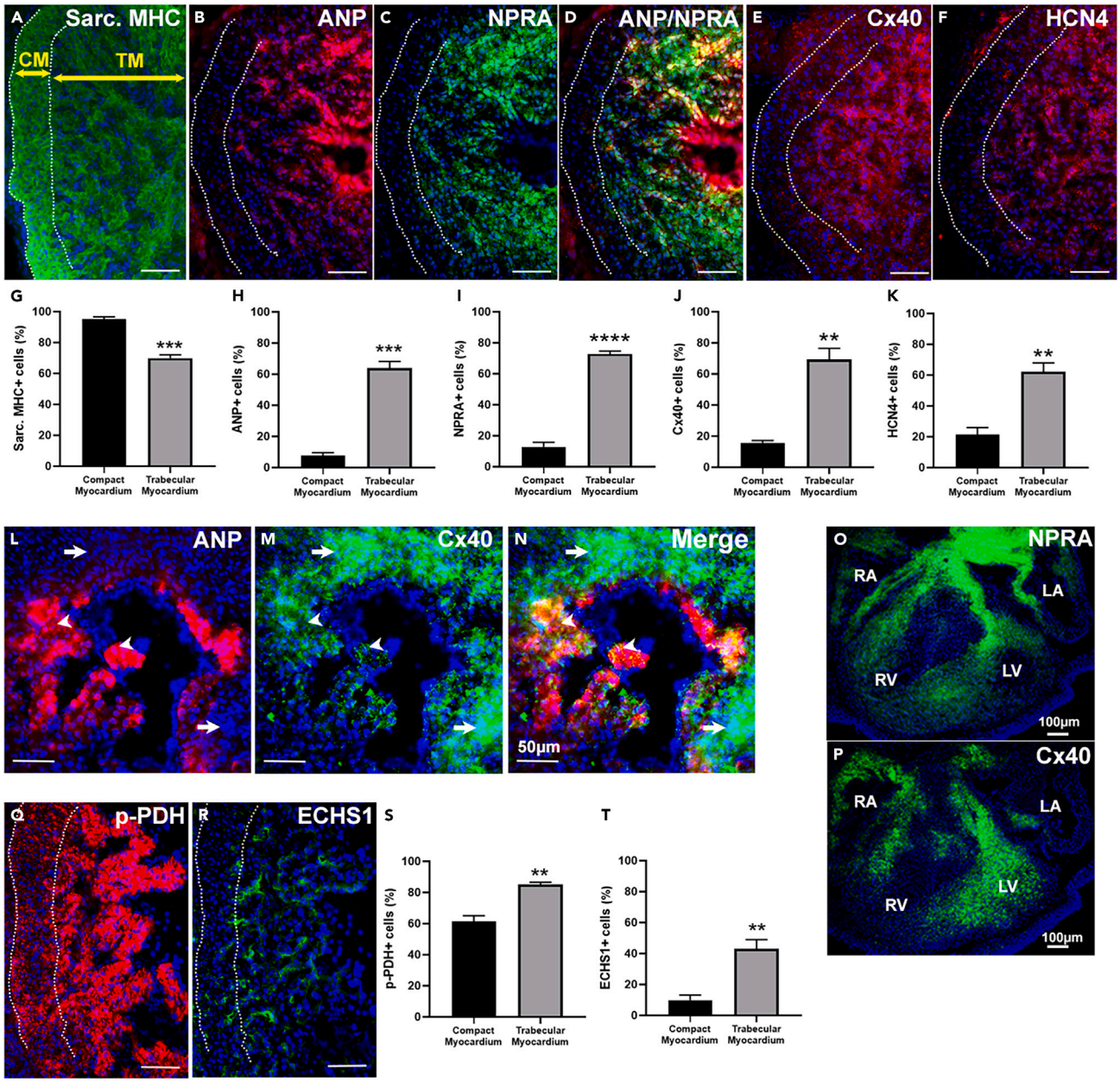

Figure 1. Immunolocalization of ANP/NPRA and markers of VCS cells and energy metabolism in the trabecular and compact myocardium of E11.5 hearts

(A–F) E11.5 left ventricular (LV) regions from parallel cardiac sections stained with Hoechst dye (blue) and antibodies specific for markers indicated on each panel. Trabecular (TM) and compact myocardium (CM) are delineated by dotted lines. (B–D) Co-immunostaining of the same section with ANP and NPRA antibodies and panel D represents a merged image. Scale bars = 50 µm.

(G–K) Quantification of cells positive for indicated markers in TM and CM. Bars represent mean ± SEM, n = 3, **p < 0.01, ***p < 0.0005, ****p < 0.0001, Student's *t* test.

(L–N) Co-immunostaining of E11.5 ventricular sections showing overlapping expression of ANP and Cx40 in TM. Arrowheads indicate cells expressing both markers and arrows indicate Cx40+ cells that are negative for ANP. Scale bars = 50 µm.

(O and P) Parallel E11.5 heart sections immunostained with NPRA and Cx40 antibodies show overlapping expression patterns in LV and RV (right ventricle). LA and RA = left and right atria, Scale bars = 100 µm.

(Q and R) Immunostaining of parallel sections for metabolic markers *p*-PDH and ECHS1. Scale bars = 50 µm.

(S and T) Quantification of cells positive for phospho-PDH and ECHS1 in TM and CM. Bars represent mean ± SEM, n = 3, **p < 0.01, Student's *t* test.

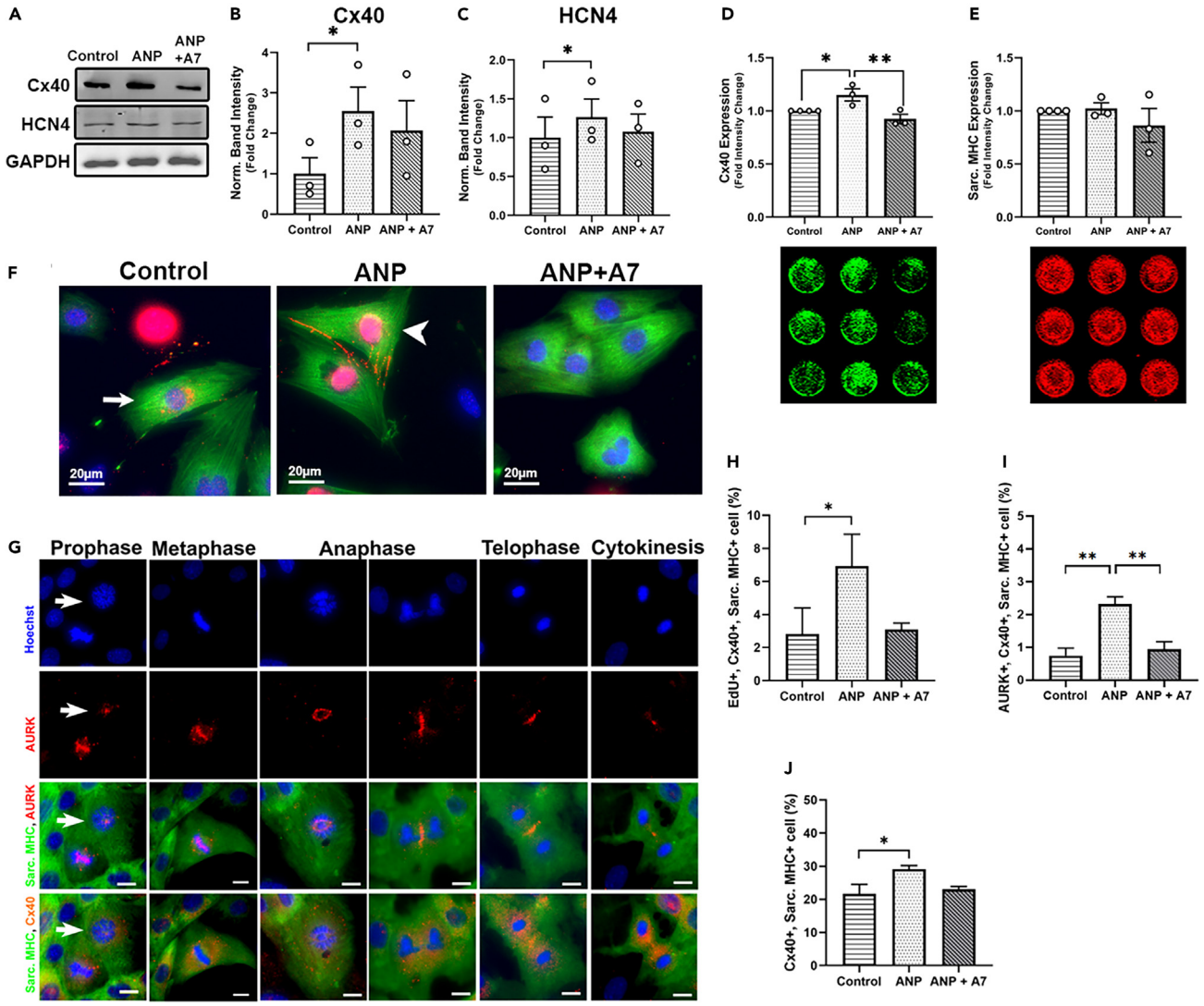

Figure 2. ANP increases VCS marker expression and cell proliferation in E11.5 ventricular cell cultures

(A) Representative western blots for Cx40, HCN4 and GAPDH levels in E11.5 ventricular cell cultures treated with or without ANP and or NPRA inhibitor (A71915 or A7) for 3 days.

(B and C) Quantification of Cx40 and HCN4 expression levels normalized to that of GAPDH. Levels in treated groups are presented as fold changes compared to the control group. Bars represent mean ± SEM, n = 3, *p < 0.05, One-way ANOVA, Dunnett's multiple comparisons test.

(D and E) In-cell western analysis of Cx40 and sarc. myosin levels in E11.5 ventricular cell cultures treated with or without ANP and NPRA inhibitor (A7) for 1 day. Bars represent mean ± SEM, n = 3–4, *p < 0.05, **p < 0.01, One-way ANOVA, Dunnett's multiple comparisons test.

(F) Click-IT EdU nuclear labeling of cultures treated with or without ANP and A7. VCS cardiomyocytes (Cx40+Sarc. MHC+) were identified by co-staining with Cx40 and sarc. MHC antibodies. Arrow indicates a Cx40+ VCS cardiomyocyte negative for Edu labeling and arrowhead indicates an Edu labeled VCS cardiomyocyte. Note the Cx40 localization in the plasma membrane of two adjacent non-dividing cells.Scale bars = 20μm.

(G) Examples of VCS cells undergoing cell division in cultures treated with ANP. Mitotic figures and cell division were visualized by pan-phospho-aurora kinase (AURK) immunostaining and Hoechst nuclear staining. VCS were cells identified using antibodies for sarcomeric MHC and Cx40. Note the cytoplasmic localization of Cx40 in VCS cells undergoing mitosis and cytokinesis. Scale bars = 20 μm.

(H–J) Percentage distribution of EdU labeled (H), AURK+ (I) and total (J) VCS cardiomyocytes in E11.5 ventricular cell culture treated with or without ANP and A7 for 1 day. Bars represent mean ± SEM, n = 3, *p < 0.05, **p < 0.01, One-way ANOVA, Dunnett's multiple comparisons test.

consistently co-localized with the mitotic figures as visualized by Hoechst staining (Figure 2G). Notably, Cx40 staining was frequently seen on the cell membrane as well as in the intracellular compartments in VCS cells positive for Edu labeling (Figure 2F). Whereas Cx40 staining appeared predominantly in the intracellular locations in VCS cells undergoing mitosis (Figure 2G). At the same time, the percentage of Cx40 expressing cardiomyocytes (Cx40+Sarc. MHC+) was also significantly higher in ANP treated cultures compared to control cultures

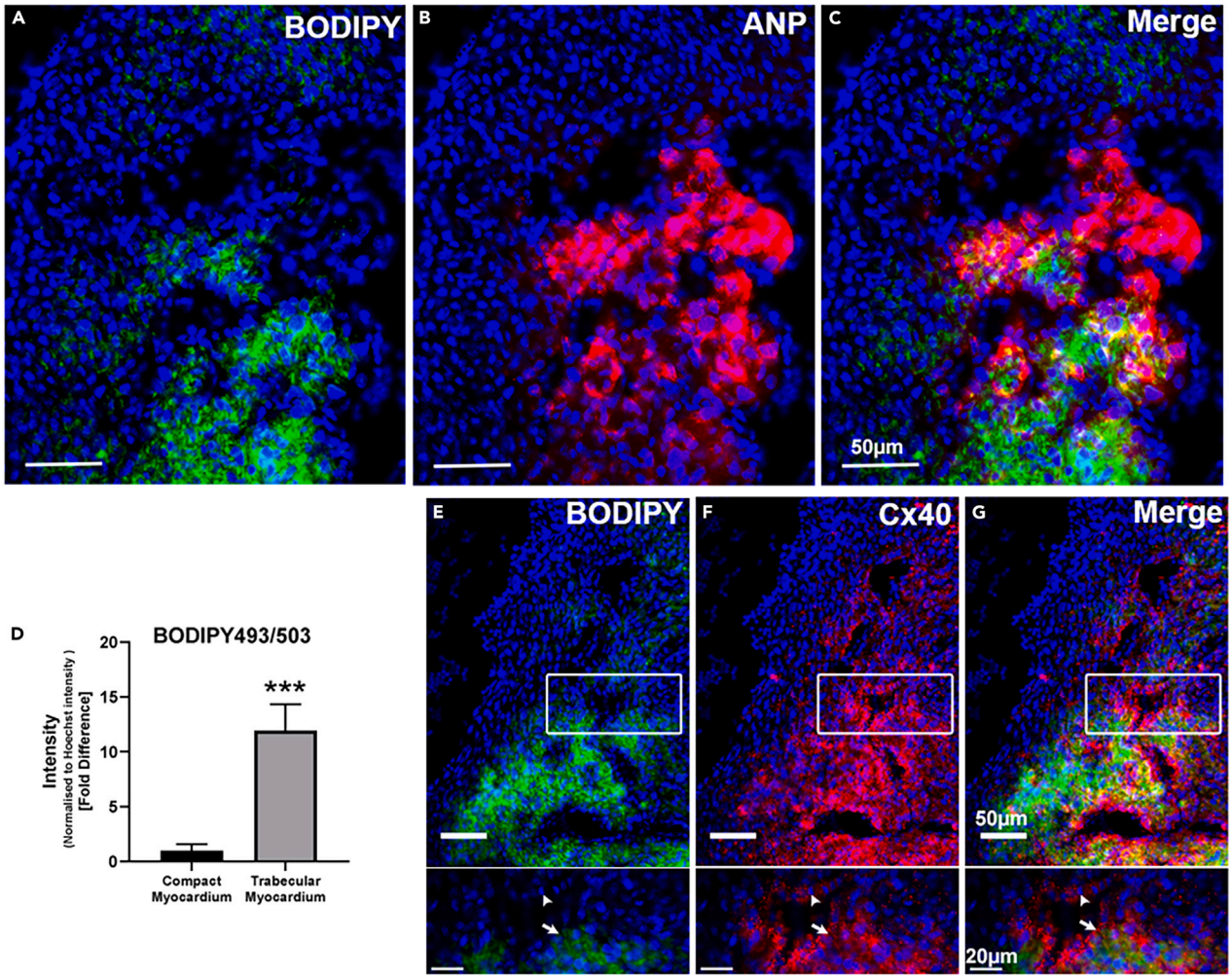
A
BODIPY
B
ANP
C
Merge
50μm
D
BODIPY493/503
Intensity
(Normalised to Hoechst intensity)
[Fold Difference]
***
Compact Myocardium
Trabecular Myocardium
E
BODIPY
F
Cx40
G
Merge
50μm
20μm
H
Control
20μm
I
Sarc. MHC, BODIPY
ANP
20μm
J
A7+ANP
20μm
K
BODIPY Intensity
(Fold Change)
***
*
Control
ANP
ANP + A7
L
BODIPY+, Sarc. MHC+ cells (%)
**
Control
ANP
ANP+A7
M
Normalized Area
*
***
DG
TG
Lipid class
Control
ANP
A7+ANP

Figure 3. ANP regulates lipid storage dynamics and Cx40 expression in the embryonic heart

(A–C) E11.5 heart sections co-stained with BODIPY 493/503 (BODIPY) and anti-ANP antibody to visualize the lipid droplets (LDs, green) (A) and ANP (B) in the CM and TM. (C) merged image demonstrates a correlation between ANP and lipid droplets. Scale bar = 50 μm.

(D) Quantification of BODIPY fluorescence intensities normalized to Hoechst fluorescence in TM and CM. Bars represent mean ± SEM, n = 3, ***p < 0.0005, Student's unpaired *t* test.

(E–G) Co-labelling with BODIPY and Cx40 antibodies to visualize LDs and Cx40 expression. Arrows indicate cells positive for Cx40 storing LDs, whereas arrowheads indicate Cx40 expressing cells without LDs in magnified boxes. Scale bar = 50 μm (overviews) and 20 μm (magnified boxes).

(H–J) Images showing lipid accumulation in E11.5 ventricular cell cultures treated with or without ANP and A7 for 3 days. Cells are co-labelled with BODIPY (green), Sarc. MHC (red) and Hoechst (blue). Scale bars = 20 μm.

(K and L) Quantification of BODIPY fluorescence intensities normalized to Hoechst fluorescence (K) and percent distribution of lipid storing cardiomyocytes (BODIPY + sarc. myosin+, L) in E11.5 ventricular cell cultures treated with or without ANP and A7. Bars represent mean ± SEM, n = 3, *p < 0.05, **p < 0.01, ***p < 0.0005, One-way ANOVA, Dunnett's multiple comparisons test.

(M) Lipidomic analysis of diglyceride (DG) and triglyceride (TG) lipid classes in E11.5 ventricular cells treated with or without ANP for 3 days. Each dot represents an individual fatty acyl lipid species and bars represent total mass. All statistical comparisons were performed pairwise, and log scaled. Wilcoxin signed rank test with Bonferroni correction was used to determine the significance of a median pairwise fold-increase in lipid amounts at an overall significance level of 5%.

(~1.3-fold, Figure 2J). Although ANP+A7 co-treatment reversed the stimulatory effect of ANP on AURK+ VCS cell (Cx40+Sarc. MHC+) numbers, such a reversal was not observed with EdU+ and overall VCS cell numbers (Figures 2H–2J). However, compared to control cultures, both ANP or ANP+A7 treated cultures did not reveal any significant effects on Cx40 negative and Sarc. MHC+ cell type in terms of their percent distribution and Edu or AURK labeling (Data S2A and S2B). Taken together, these results suggest that ANP treatment can increase the cell cycle activity and the number of Cx40+ VCS myocytes in E11.5 ventricular cell cultures but the co-treatment with A7 is unable to fully reverse these stimulatory effects of ANP.

ANP promotes lipid droplet storage in the embryonic heart

The neutral lipid content in E11.5 ventricular sections was visualized using a fluorescent dye BODIPY493/503 (BODIPY) which stains lipid droplets (LDs). LDs are storage organelles which contain a neutral lipid core (triglycerides: TG and sterol esters) surrounded by a phospholipid monolayer. Co-staining of sections with ANP antibodies and BODIPY revealed overlapping areas of ANP expression and LDs in the TM (Figures 3A–3C). A significant difference in LD storage was observed between TM and CM. Upon quantification and normalization to Hoechst intensity, BODIPY stained area was 12-fold higher in the TM compared to the CM. (Figure 3D). Further, co-staining of sections with Cx40 antibodies and BODIPY also revealed overlapping areas of Cx40 and LD storage predominantly in the TM (Figures 3E–3G). Although Cx40 expressing areas are rich in LDs, not all Cx40 expressing cells show LD storage. The effect of ANP on LD accumulation in the embryonic ventricles was further corroborated in primary culture experiments (Figures 3H–3J), wherein BODIPY staining intensity was significantly higher in E11.5 ventricular cells treated with ANP for 3 days compared to the untreated control and ANP+A7 co-treated groups (Figure 3K). In addition, the percentage cardiomyocytes positive for LDs was also significantly higher in ANP treated cultures compared to the control cultures (Figure 3L).

LDs can undergo intracellular lipolysis to release fatty acids for energy production and membrane synthesis. Lipidomic analysis was performed to assess if lipid profiles are altered in response to ANP/NPRA signaling. Notably, ventricular cells treated with ANP revealed a significant decrease in TG levels with a concomitant increase in diglyceride (DG) levels compared to control cultures (−0.7-fold and 1.3-fold for TG and DG respectively, ANP vs. control, Figure 3M). The increase in DG and decrease in TG are consistent with LDs being metabolically active and converting TG to DG and free fatty acids. In addition, significant increases in the levels of lysophosphatidylcholine (LPC), phosphatidylglycerol (PG) and sphingomyelin (SM) were also observed in ANP treated cells (Data S3). Surprisingly, ANP+A7 group did not show any changes in DG and TG levels compared to ANP treatment (Figure 3M). Also, ANP+A7 but not ANP treatment affected the levels of ceramides and phosphatidylethanolamine (Data S3). Collectively, these results suggest that ANP/NPRA signaling can increase lipid uptake, LD formation and metabolism and Cx40 expression in a subset of embryonic ventricular myocytes.

Fatty acid supplementation and exogenous ANP show additive effects on lipid droplet formation and VCS cell differentiation

To directly test the effect of increased lipid droplet metabolism on Cx40+ cell numbers, E11.5 ventricular cell cultures were supplemented with varying concentrations of the free fatty acids oleic acid (OA) and linoleic acid (LA) conjugated with bovine serum albumin (BSA) for 3 days. Both types of fatty acid treatments significantly increased the percentage of BODIPY positive cells in a dose dependent manner (Figures 4A and 4B). Cultures treated with either OA or LA (400μM) revealed significant increases in the percentages of Cx40 expressing cells (2.1-fold, 2-fold for OA and LA respectively) and LD storing cells (2.7-fold, 2.3-fold for OA and LA respectively) compared to the BSA treated control groups (Figures 4A and 4B). Further, there was a strong positive correlation between the percentages of Cx40 expressing cells and BODIPY positive cells in OA or LA supplemented cell cultures (Figures 4A and 4B). Co-staining for Cx40 and BODIPY (Figures 4C–4E) indicated that the majority of LD storing cells (~70–90%) were also positive for Cx40 irrespective of OA or LA concentration in cell culture medium (Figure 4F). However, only ~40–70% Cx40 expressing cells showed LDs storage under the conditions described (Figure 4G).

Subsequently, combination of lower concentrations of OA and LA (200μM each) were used to test the effects on Cx40 gene expression using RT-qPCR analysis. Cx40 mRNA expression was increased by 2.1-fold in OA + LA treated cultures compared to the BSA controls after 1-day treatment (Figure 4H). In-cell westerns and immunostaining experiments also showed a significant increase in the total Cx40 expression

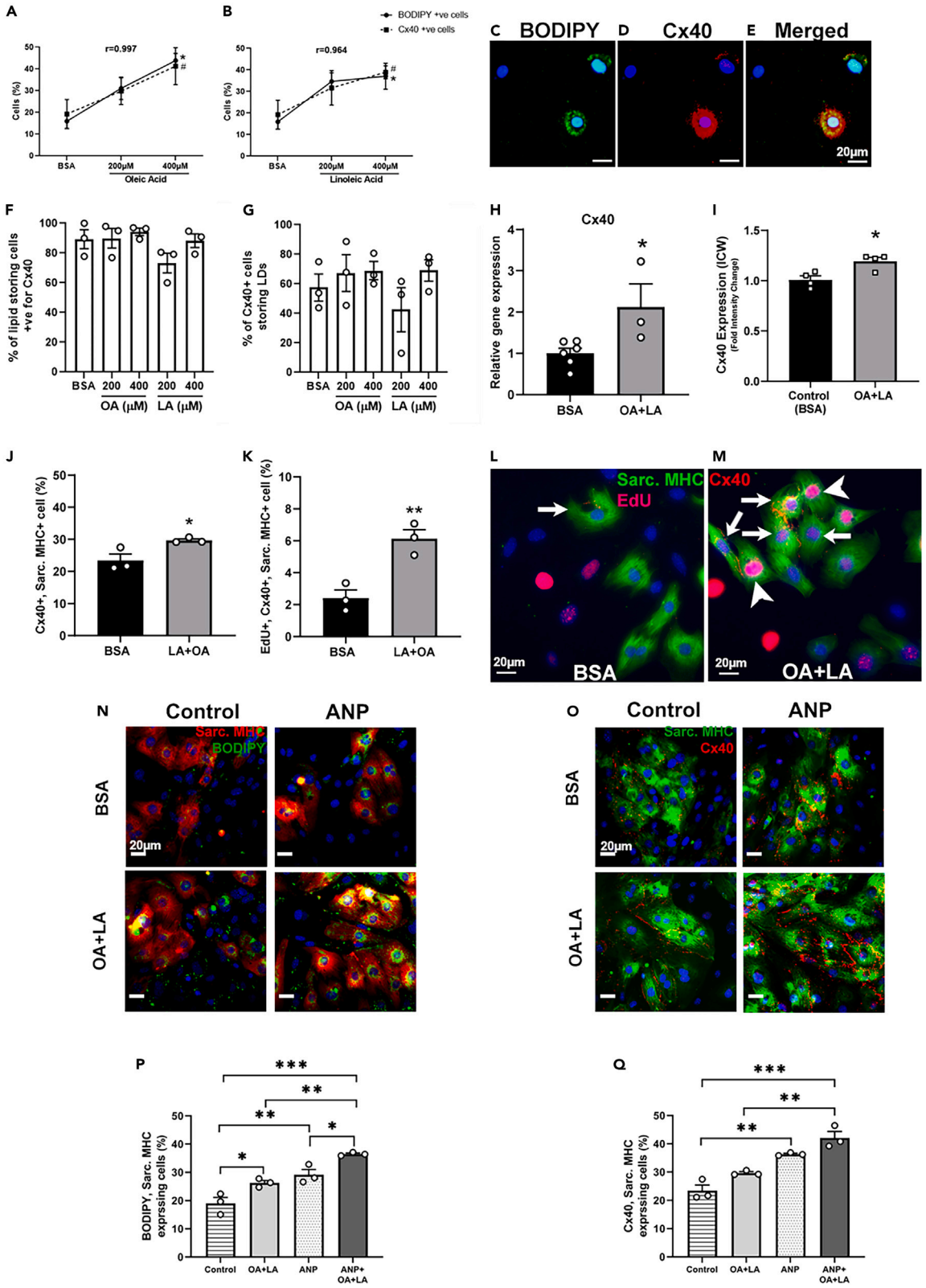
A
r=0.997
Cells (%)
BSA
200μM
400μM
Oleic Acid
B
BODIPY +ve cells
Cx40 +ve cells
r=0.964
Linoleic Acid
C BODIPY
D Cx40
E Merged
20μm
F
% of lipid storing cells +ve for Cx40
OA (μM)
LA (μM)
G
% of Cx40+ cells storing LDs
H
Cx40
Relative gene expression
I
Cx40 Expression (ICW)
(Fold Intensity Change)
Control (BSA)
OA+LA
J
Cx40+, Sarc. MHC+ cell (%)
LA+OA
K
EdU+, Cx40+, Sarc. MHC+ cell (%)
L
Sarc. MHC
EdU
BSA
M
Cx40
OA+LA
N
Control
ANP
Sarc. MHC
BODIPY
O
P
BODIPY, Sarc. MHC exprssing cells (%)
ANP
ANP+ OA+LA
Q
Cx40, Sarc. MHC exprssing cells (%)

Figure 4. Additive effects of fatty acid and ANP supplementation on lipid droplet formation and VCS cell differentiation

(A and B) Correlation analysis of LD storing cells (BODIPY+) and Cx40 expressing cells in cultures treated with different concentrations of oleic acid (A) and Linoleic acid (B). n = 3, *p < 0.05 (BSA control vs. 400μM OA or LA, BODIPY+ cells), #p < 0.05 (control vs. 400μM OA or LA, Cx40+ cells), two-way ANOVA, Tukey's multiple comparisons test, r = Pearson correlation coefficient between Cx40+ cells and lipid storing cells.

(C–E) Representative images showing cells co-labelled with BODIPY, Cx40 and Hoechst in E11.5 ventricular cell culture treated with OA and LA for 3 days.

(F and G) Percent distribution of lipid-storing cells with Cx40 expression (F) or Cx40+ cells with LD storage in fatty acid supplemented E11.5 ventricular cell cultures. n = 3, no significant differences between groups.

(H and I) Relative levels of Cx40 gene expression (H) and Cx40 protein (I, In-cell western) in E11.5 ventricular cell culture treated with OA and LA (200μM each) compared to the control (BSA) group. Bars represent mean ± SEM, n = 3, *p < 0.05, Student's unpaired *t* test.

(J and K) Percentage distribution of Cx40+ cardiomyocytes (J) and EdU labeled Cx40+cardiomyocytes (K) in E11.5 ventricular cell culture treated with or without fatty acids for 1 day. Bars represent mean ± SEM, n = 3, *p < 0.05, **p < 0.005, Student's unpaired *t* test.

(L and M) Representative images to compare the effect of fatty acids (OA + LA) on Cx40+cardiomyocyte (Cx40+Sarc. MHC+) proliferation by Click-IT EdU nuclear labeling. Arrows indicate Cx40+ cardiomyocytes and arrowheads indicate Edu labeled (proliferating) Cx40+ cardiomyocytes. Scale bars = 20μm.

(N and O) Representative immunostained images demonstrating the additive effect of ANP and fatty acids on LDs storage (green; N) and Cx40 expression (red; O) by staining with BODIPY for LDs and Cx40 antibodies. Cardiomyocytes are labeled with Sarc. MHC antibodies (red in panel N and green in panel O). Scale bars = 20μm.

(P and Q) Percentage distribution of lipid storing cardiomyocytes (P) and Cx40 expressing cardiomyocytes (Q) in E11.5 ventricular cell culture treated with fatty acids, ANP and a combination of ANP and fatty acids. Bars represent mean ± SEM, n = 3, *p < 0.05, **p < 0.01, ***p < 0.0005, One-way ANOVA, Tukey's multiple comparisons test.

levels (Figure 4I) as well as the percentage of cells positive for both Cx40 and Sarc. MHC (Figure 4J) after OA + LA treatment for 3 days. Notably, the cell proliferation rate of Cx40+/Sarc. MHC+ cells was also significantly increased in OA + LA treated cell cultures (2.5-fold vs. BSA control, Figures 4K–4M). These results suggest that FA supplementation can mimic ANP effects on VCS marker expression and cell proliferation in E11.5 ventricular cell cultures.

Next, the combined effect of ANP and FA supplementation on neutral lipid storage and VCS cell number was assessed in E11.5 ventricular cells (Figures 4N and 4O). Cultures co-treated with ANP and OA + LA revealed a significantly higher percentage of lipid storing cardiomyocytes compared to the control and ANP or OA + LA only treated groups (1.9-fold vs. control, 1.2-fold vs. ANP only and 1.4-fold vs. OA + LA only; Figure 4P). This result further indicates that ANP treatment can stimulate fatty acid uptake as well as lipid storage in the embryonic heart. Additional immunostaining analyses revealed a significantly higher percentage of Cx40 positive cardiomyocytes in cultures co-treated with ANP and OA + LA compared to the control and ANP or OA + LA only treated groups (1.8-fold vs. control, 1.2-fold vs. ANP only and 1.4-fold vs. OA + LA only, Figure 4Q). Overall, these data indicate the involvement of ANP mediated intracellular lipid accumulation in the regulation of VCS cell differentiation during embryonic heart development.

Effects of ANP on metabolic events in embryonic ventricular cells

Higher levels of lipid content and metabolic markers (phospho-PDH and ECHS1) in the TM compared to the CM (Figure 1) suggest that trabecular cells may have more functional mitochondria to assist with oxidative phosphorylation compared to the CM. In order to distinguish regional differences in mitochondrial function, unfixed cryosections from E11.5 hearts were stained with JC-10 dye which forms a red fluorescent aggregates in mitochondria with an active membrane potential[33,34] (Figure 5A). Quantification of fluorescence intensities revealed a significantly higher red fluorescence signal in the TM compared to the CM (17.6-fold, Figure 5B).

Subsequently, the effects of ANP on cellular metabolism in E11.5 ventricular cell cultures was examined using seahorse assays (Figures 5C and 5D). Since, glucose is the predominant source of energy in the embryonic heart,[17,35] the first set of metabolic assays were performed on cells treated with or without ANP for 24 h and subsequently switched to substrate limited DMEM supplemented with 10 mM glucose for 1h prior to seahorse recordings as reported earlier.[36] A significant increase in the basal level of glycolysis was observed in cultures treated with ANP by measuring extracellular acidification rate (ECAR; 1.9-fold vs. control and 2.2-fold vs. ANP+A7; Figure 5E). Glycolytic capacity was also significantly increased in ANP treated cultures upon injection with oligomycin (an ATP synthase inhibitor; 1.9-fold vs. control and 2.3-fold vs. ANP+A7; Figure 5F). In addition, the basal oxygen consumption rate (OCR) was significantly higher in ANP treated cultures (2.1-fold vs. control and 5.1-fold vs. ANP+A7, Figure 5G). Similarly, the maximal OCR after FCCP treatment was also significantly higher in ANP treated cultures (1.7-fold vs. control and 3.7-fold vs. ANP+A71915, Figure 5H). Further analysis of ECAR/OCR ratios revealed that ANP/NPRA pathway can promote a shift in the energy metabolism from a relatively low energy state to a high energetic state by stimulating both anerobic and aerobic pathways in E11.5 ventricular cells (Figure 5I).

Although fatty acid usage for energy production is relatively much lower in the embryonic and fetal hearts compared to the postnatal hearts,[37–39] presence of BODIPY positive neutral LDs and the shift from TG to DG which would release free fatty acids in E11.5 ventricular cells suggests an increase in FAO capacity. To examine whether ANP has any effect on fatty acid utilization by β-oxidation, E11.5 cell cultures were maintained in substrate limited DMEM supplemented with 0.5 mM glucose and 0.5 mM carnitine and treated with or without ANP for 24 h. Subsequently, cells were switched to FAO buffer for 1 h and supplemented with OA + LA BSA conjugates just before taking measurements. Seahorse assay results revealed a significant increase in basal OCR (indicative of basal FAO) in ANP treated cultures (1.3-fold vs. control and 2.2-fold vs. ANP+A7, Figure 5J). Maximal OCR (maximal FAO) was also significantly higher in ANP treated (1.2-fold vs. control and 2.1-fold vs. ANP+A71915, Figure 5K). These results suggest that ANP can promote utilization of both glucose and fatty acids for mitochondrial energy metabolism in E11.5 ventricular cells.

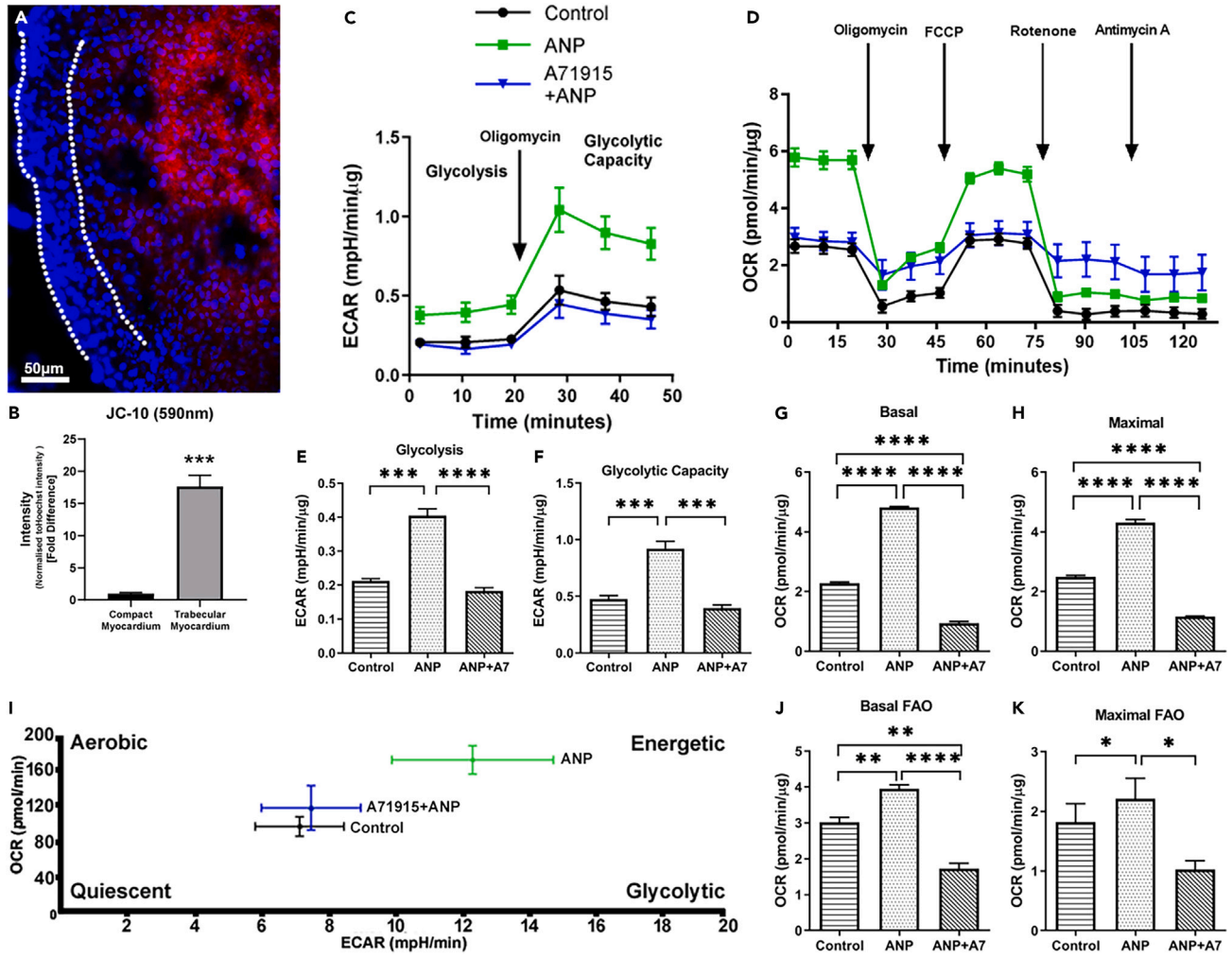

Figure 5. Effects of ANP on metabolic events in embryonic ventricular cells

(A) JC-10 staining of an unfixed E11.5 ventricular cross section to monitor the mitochondrial membrane potential in compact (CM) and trabecular (TM) regions. Scale bar = 50µm.

(B) Quantification of JC-10 (590nm) fluorescence intensities normalized to Hoechst fluorescence in TM and CM. Bars represent mean ± SEM, n = 3, ***p < 0.0005, Student's unpaired *t* test.

(C and D) Representative traces of extracellular acidification rates (ECAR, C) and oxygen consumption rates (OCR, D). E11.5 ventricular cell cultures treated with or without ANP and A71915 in 10%FBS-DMEM for 24 h. After this period, the medium was replaced with substrate limited DMEM supplemented with 10mM glucose, 1mM pyruvate and 2mM glutamine for 1 h prior to performing seahorse assays as described in STAR Methods.

(E and F) Analysis of ECAR to assess the changes in glycolysis (E) and glycolytic capacity (F) in E11.5 ventricular cell cultures treated with or without ANP and A71915. ECAR values were normalized to the total protein. Bars represent mean ± SEM, n = 3, ***p < 0.0005, ****p < 0.0001. One-way ANOVA, Tukey's multiple comparisons tests.

(G and H) Analysis of OCR in cell culture to demonstrate changes in basal (G) and maximal (H) mitochondrial oxidative phosphorylation by ANP. OCR values were normalized to the total protein. Bars represent mean ± SEM, n = 3, ****p < 0.0001. One-way ANOVA, Tukey's multiple comparisons tests.

(I) OCR/ECAR ratio to demonstrate the shift of metabolism from a relatively quiescent stage to a higher energy metabolic state by ANP in embryonic ventricular cells.

(J and K) Analysis of fatty acid oxidation (FAO) in E11.5 ventricular cell cultures treated with or without ANP and A71915. seahorse assay shows increased OCR in ANP-treated cell culture. Bars represent mean ± SEM, n = 3, *p < 0.05, **p < 0.01, ****p < 0.0001. One-way ANOVA, Tukey's multiple comparisons tests.

ANP treatment affects gene expression of key metabolic markers, transcriptional regulators and histone acetylation in embryonic ventricular cells

Consistent with an increase in ECAR, cells treated with ANP revealed a significant increase in the mRNA levels of lactate dehydrogenase A (LDHA) but not LDHB (1.6-fold vs. control, Figure 6A). In addition, gene expression levels of pyruvate dehydrogenase kinase 4 (PDK4) also increased after ANP treatment (1.4-fold vs. control, Figure 6B). Gene expression levels of other enzymes such as pyruvate dehydrogenase (PDHA1) and PDH phosphatase (PDP1) were not significantly altered in ANP treated cultures (Figure 6B). Consistent with an increase in

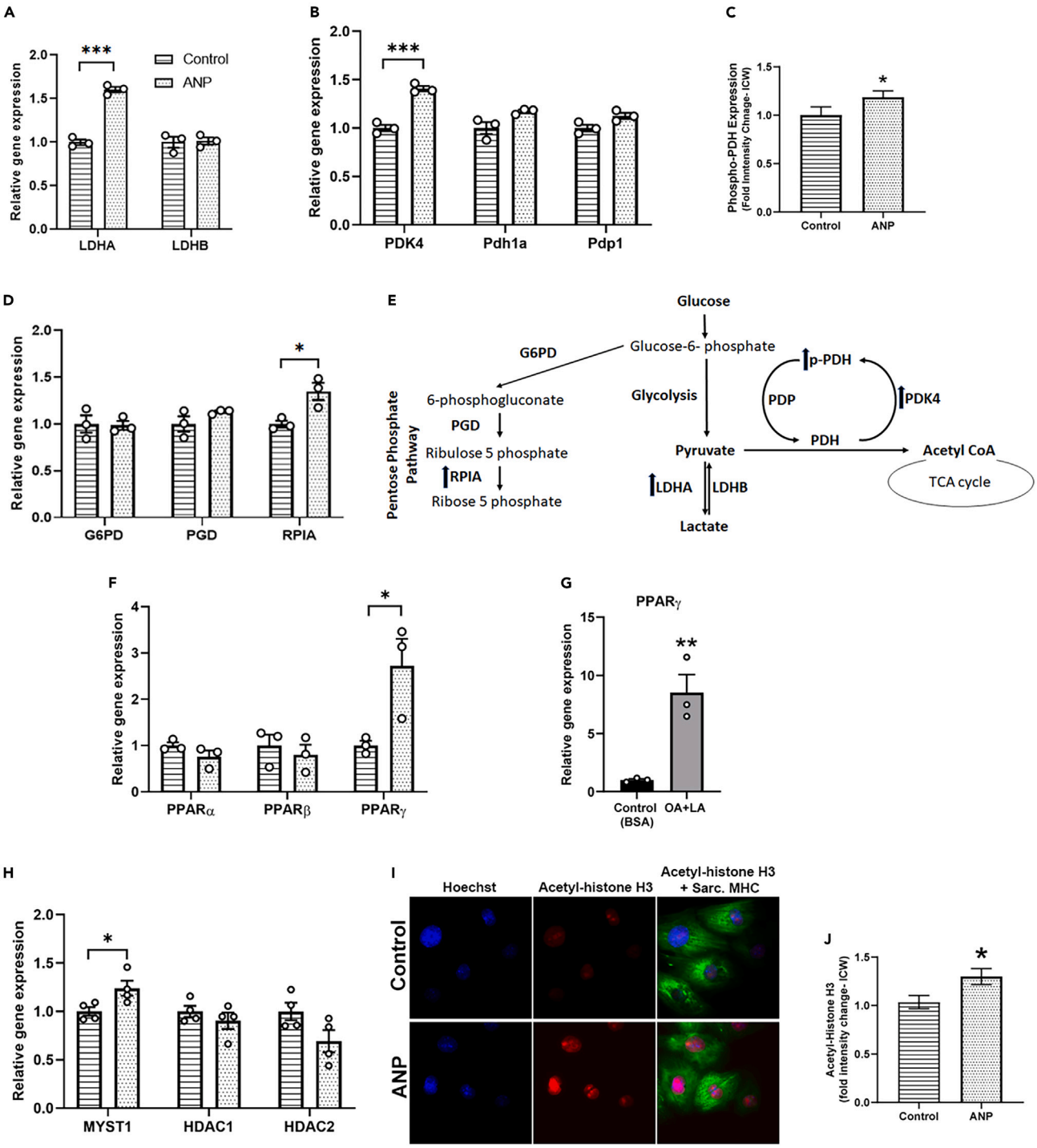

Figure 6. ANP treatment affects gene expression of key metabolic markers, transcriptional regulators and histone acetylation in E11.5 ventricular cell cultures

(A) Gene expression of lactose dehydrogenase A and B (LDHA and LDHB) in cultures treated with or without ANP. Bars represent mean ± SEM, n = 3, ***p < 0.0005, Student's unpaired *t* test.

(B) Gene expression of pyruvate dehydrogenase kinase 4 (PDK4), pyruvate dehydrogenase (Pdh1a), and pyruvate dehydrogenase phosphatase (Pdp1) in E11.5 cultures treated with or without ANP. Bars represent mean ± SEM, n = 3, ***p < 0.0005, Student's unpaired *t* test.

(C) In-cell western analysis of expression of *p*-PDH in cultures treated with or without ANP. Bars represent mean ± SEM, n = 3, *p < 0.05, Student's unpaired *t* test.

Figure 6. *Continued*

(D) Gene expression of glucose-6-phosphate dehydrogenase (G6PD), 6-phosphogluconate dehydrogenase (PGD) and ribose 5-phosphate isomerase (RPIA) in E11.5 cultures treated with or without ANP. Bars represent mean ± SEM, n = 3, *p < 0.05, Student's unpaired *t* test.

(E) A schematic representation showing the role of LDHA, LDHB, PDK4, Pdh1a and Pdp1 in relation to glucose oxidation as well as the role of G6PD, PGD and RPIA in relation to pentose phosphate pathway.

(F and G) Gene expression of PPARα, β and γ in E11.5 ventricular cell cultures treated with or without ANP (F) and fatty acids (OA + LA; G). Bars represent mean ± SEM, n = 3, *p < 0.05, **p < 0.01Student's unpaired *t* test.

(H) Gene expression of MYST1, HDAC1 and 2 in E11.5 ventricular cells cultures treated with or without ANP. Bars represent mean ± SEM, n = 3, *p < 0.05, Student's unpaired *t* test.

(I) Representative images of cells immuno-stained with antibodies specific for acetylated histone H3 and Sarc. MHC. in cultures treated with or without ANP.

(J) In-cell western analysis of histone H3 acetylation in E11.5 ventricular cell cultures treated with or without ANP. Bars represent mean ± SEM, n = 3, *p < 0.05, Student's unpaired *t* test.

PDK4 levels, in-cells westerns revealed a slight but significant upregulation of phospho-PDH (*p*-PDH) protein levels in ANP treated cells (1.2-fold vs. control, Figure 6C). Upregulated glycolysis is likely to promote the pentose phosphate pathway (PPP) in proliferating cells.[40,41] To analyze whether ANP treatment can regulate the expression levels of enzymes involved in PPP, relative gene expression levels of Glucose-6-phosphate dehydrogenase (G6PD), 6-phosphogluconate dehydrogenase (PGD) and ribose 5-phosphate isomerase (RPIA) were determined by RT-qPCR analysis. The expression levels of G6PD and PGD did not change significantly, however RPIA expression was significantly increased with ANP treatment (1.35-fold vs. control, Figure 6D). Since fatty acids are natural ligands for the members of peroxisome proliferator-activated receptor family (PPAR-α, β and γ), we reasoned that PPARs may be responsible for ANP effects on lipid metabolism and VCS marker gene expression. RT-qPCR analysis revealed that gene expression of PPARγ but not PPARα or PPARβ was upregulated in ANP treated E11.5 ventricular cell cultures compared to controls (2.7-fold, Figure 6E). Likewise, OA + LA cocktail had even greater increase in PPARγ mRNA expression (8.5-fold) compared to the BSA control (Figure 6G). These results indicate that PPARγ may play an important role in VCS marker gene expression.

Citrate generated in the tricarboxylic acid cycle (TCA) can be exported to the cytosol or nucleus via citrate shuttle and is converted to acetyl CoA which can in turn increase protein acetylation and regulate gene expression.[42] Based on the stimulatory effects of ANP on both aerobic and anaerobic metabolic events in E11.5 cells, its effect on histone acetylation was assessed by RT-qPCR, immunocytochemistry, and in-cell westerns (Figures 6H–6J). Gene expression of histone acyltransferase (MYST1) was upregulated in ANP treated cultures (1.2-fold vs. control, Figure 6H), whereas gene expression levels of histone deacetylase 1 and 2 (HDAC1 and 2) were not altered significantly (Figure 6H). Immunostaining and in-cell western analysis revealed a significant increase in acetylated histone H3 levels in ANP treated cell cultures compared to the untreated control cultures (1.3-fold, Figures 6I and 6J). These data suggest that stimulatory effects of ANP on cellular metabolism could lead to increases in VCS marker gene expression via epigenetic changes and histone acetylation.

Role of PPARγ and fatty acid oxidation in ANP mediated regulation of Cx40 expression

The role of PPARγ in Cx40 expression was assessed in E11.5 ventricular cultures treated with or without ANP and or a PPARγ specific inhibitor (GW9662). In-cell western analysis revealed that Cx40 expression was significantly decreased in E11.5 ventricular cell cultures treated with GW9662 alone (0.5 μM) for 3 days compared to the vehicle control. Similarly, PPARγ inhibition also reduced Cx40 expression levels in cultures co-treated with ANP and GW9662 compared to the levels in cultures treated with ANP (Figure 7A). Likewise, PPARγ inhibition also reduced Cx40 expression levels in cultures co-treated with OA + LA and GW9662 compared to the levels in cultures treated with OA + LA alone (Figure 7B). Collectively these results indicate a critical role for PPARγ in the regulation of CX40 expression in embryonic ventricular cells treated with ANP and fatty acids.

Next, the effect of inhibition of FAO on Cx40 expression was assessed in E11.5 ventricular cell cultures treated with or without ANP and or Etomoxir (2.5μM, an inhibitor of CPT1 which transports fatty acids to the mitochondria). In-cell western experiments reveled a significant increase in Cx40 expression in ANP treated cultures compared to control or Etomoxir treatment alone (Figure 7C), However, ANP mediated increase in Cx40 expression was significantly reduced in cultures co-treated with ANP and Etomoxir (Figure 7C; 38% difference in Cx40 expression between ANP+ETO and ANP only culture groups). E11.5 cell cultures co-treated with ANP and etomoxir also revealed a significant reduction in Sarc. MHC expression by in-cell western analysis (Figure 7D). Overall, these data show that FAO is critical in Cx40 expression and dysregulation of FAO may cause defects in VCS development.

DISCUSSION

Although the effects of ANP on lipid metabolism and lipolysis are documented in other tissues,[25] to our knowledge, this is the first report describing a critical role for ANP in the regulation of lipid droplet accumulation and overall energy metabolism in VCS cell proliferation and differentiation. While previous reports described the coincidence of ANP and Cx40 expression during VCS development,[10,14] results from this study confirm a definitive role for ANP/NPRA signaling in promoting Cx40 expression via metabolic alterations in VCS cells. Stimulation of glycolysis or inhibition of FAO prolonged cardiomyocyte cell cycle activity in postnatal cardiomyocytes.[31,43] Despite an increase in the % of Sarc. MHC+ VCS cells, there was no change in the overall Sarc. MHC levels in ANP treated cultures. This could be due to masking of the positive effect on Cx40+ and Sarc.MHC+ cells by the presence of a more abundant Cx40-and Sarc.MHC+ cell type in E11.5 ventricular cell cultures (Data S2C). Consistent with an increase in the % of Cx40+ and Sarc. MHC+ cells, there were significant increases in the Edu and AURK

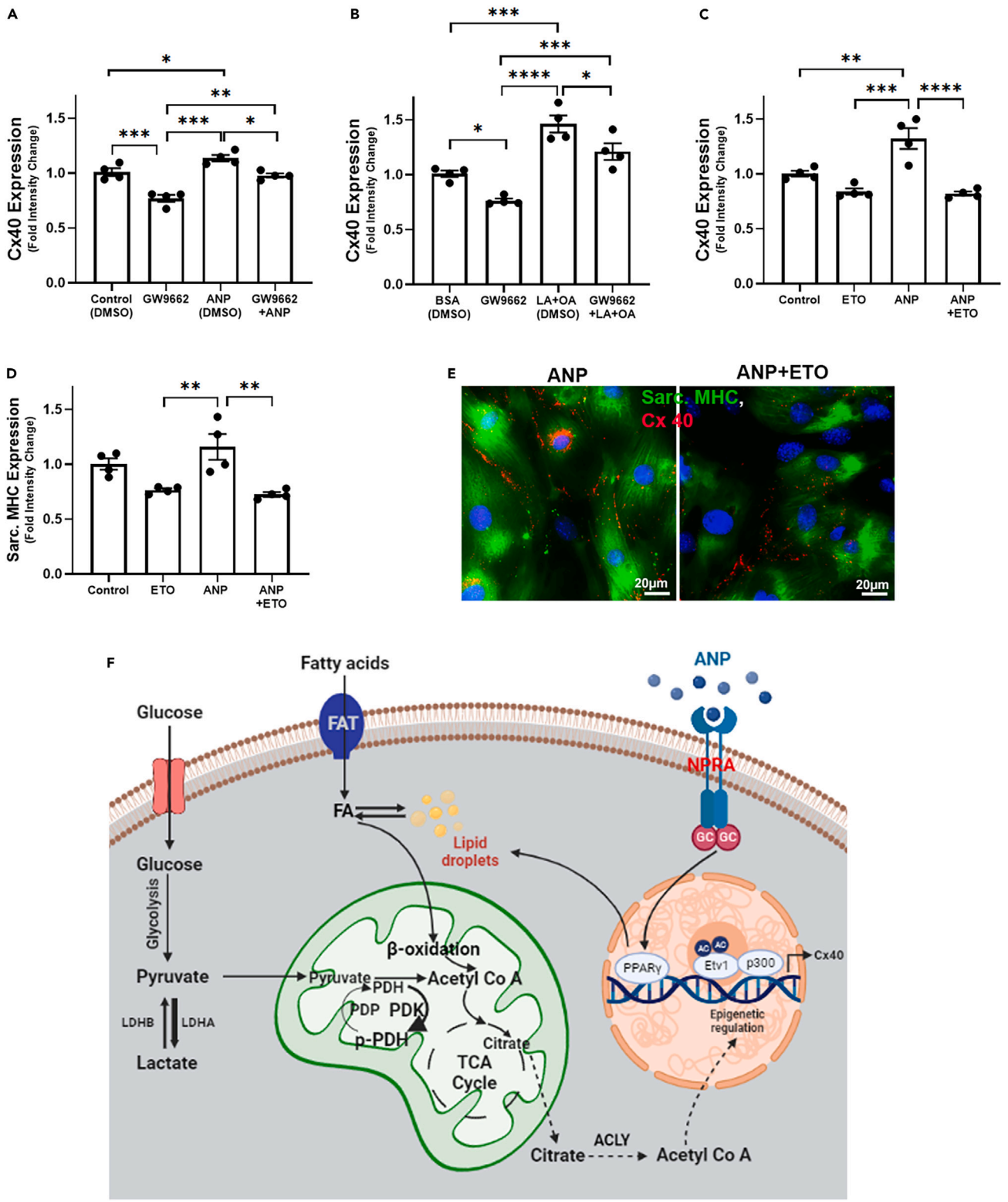

Figure 7. Role of PPARγ and fatty acid oxidation in ANP mediated regulation of Cx40 expression

(A and B) In-cell western analysis to assess the effect of PPARγ inhibitor (GW9662) on Cx40 expression in E11.5 ventricular cells treated with or without ANP (A) and with or without OA + LA (B). Bars represent mean ± SEM. n = 3, *p < 0.05, **p < 0.01, ***p < 0.0005, ****p < 0.0001. One-way ANOVA, Tukey's multiple comparisons test.

Figure 7. *Continued*

(C and D) In-cell western analysis to assess the effect of FAO inhibition in ANP treated E11.5 ventricular cell culture by Etomoxir (Cpt1 inhibitor; 2.5μM) on Cx40 expression (C) and sarc. MHC (D). Bars represent mean ± SEM. n = 3, *p < 0.05, **p < 0.01, ***p < 0.0005, ****p < 0.0001. One-way ANOVA, Tukey's multiple comparisons test.

(E) Representative immunostained images of Cx40 expressing cells cultures treated with or without ANP and etomoxir. Cells were immunolabeled with Sarc. MHC (green) and Cx40 (red). Scale Bars = 20μm.

(F) Schematic showing ANP/NPRA signaling mediated metabolic and gene expression events responsible for VCS cell differentiation in the embryonic mouse heart.

labeling of these VCS cells in ANP treated cultures. Additionally, proliferating VCS cells exhibited intracellular Cx40 staining, contrasting with plasma membrane localization in non-dividing VCS cells. The significance of this shift remains unknown, with few studies exploring Cx40 link to cell proliferation and differentiation. While increased expression of Cx40 at the plasma membrane induces endothelial cell quiescence,[44] Cx43 shows a shift from membrane to intracellular localization and altered phosphorylation during differentiation of preadipocytes and myoblasts.[45,46] In another study, Cx40.8 was found at the plasma membrane in the developing zebrafish fin, but it was retained in the Golgi apparatus during the fin regeneration.[47] Further research is needed to unravel Cx40 phosphorylation patterns, intracellular trafficking and degradation during VCS cell proliferation and differentiation.

Presence of BODIPY positive cells in E11.5 TM but not CM is likely due to stimulatory effects of ANP signaling on lipid uptake and direct access of trabecular cells to the fatty acid rich maternal blood.[48] Likewise, Cx40 expression in the majority of LD containing trabecular cells underscores the importance of lipid metabolism in VCS development. These notions are consistent with the effects of exogenous ANP and fatty acids on LD accumulation, VCS cell proliferation and marker gene expression in primary culture experiments. Absence of LDs in some Cx40-expressing cells could be attributed to complete utilization of LDs for VCS cell differentiation and is consistent with our determination that E11.5 ventricular cells are able to use fatty acids for energy generation via mitochondrial β-oxidation. Our observed decrease in TG levels with a concomitant increase in DG could be attributed to activation of neutral lipases via ANP/NPRA/PKG pathway similar to that reported in fat cells.[49] Increased FAO in this study strongly supports an important role for ANP in intracellular lipid turn over and fatty acid mobilization in E11.5 ventricular cells.

Although ANP treatment led to a significant increase in the percentage of BODIPY+/sarc. MHC+ cells compared to the control cultures, ANP+A7 treatment was not significantly different from ANP treatment alone (Figure 3L). Similarly, ANP treatment led to significant changes in TG and DG levels as well as other lipid classes compared to the control cultures, however, co-treatment with A7 did not inhibit these changes (Figure 3L and Data S2). Absence of antagonistic effects of A7 in co-treated cultures could be due to reversible competitive antagonism of A7 at NPRA receptor.[50] Since these experiments were done over a 3-day period with daily exchange of medium with fresh ANP and A7, the A7 effect could have been competed away by the fresh ligand. An alternative explanation for such a result could be due to novel actions of ANP and A7 independent of cell surface receptors. Indeed, ANP was shown to bind directly to the mitochondrial membrane in rat adrenocortical cells.[51,52] It is not known whether mitochondrial membranes in adrenocortical cells or E11.5 ventricular cells harbor NPRA like binding sites and whether A7 can also bind to such sites. Differential binding of ANP vs. A7 at such intracellular vs. extracellular target sites may explain the unexpected results observed with ANP+A7 co-treatments in this study. Further studies are required to precisely delineate mechanisms underlying dynamic lipid changes in response to ANP and A7 and their relevance to VCS cell proliferation and differentiation.

ANP treatment of E11.5 ventricular cells also led a significant increase in mitochondrial OCR in the presence of high glucose. A gradual increase in the contribution of glucose to the TCA cycle was shown in the hearts of E11.5 to E13.5 mouse embryos along with a corresponding increase in the expression of mitochondrial electron transport chain proteins.[53,54] ANP was shown to increase glucose uptake via recruitment of Glut1 and Glut4 transporters in postnatal cardiomyocytes[55] and increase glucose oxidation in adipocytes via cGMP/PKG/Akt/mTOR pathway.[56] In the absence of fully formed coronary vasculature, a hypoxia gradient is established from the epicardium to the endocardium in E11-E15 ventricles due to diffusion limits of oxygen from the chamber lumen.[57] Consistent with this hypoxia gradient, expression profiles of genes involved in glycolysis and lipid metabolism are restricted to the CM and TM respectively in mid-gestation ventricles.[58,59] Based on Randle hypothesis, higher lipid content, and ANP/NPRA signaling in the E11.5 TM could preferentially stimulate FAO in trabecular cells. Irrespective of substrate availability, the E11.5 TM cells were reported to consist of higher mitochondrial numbers compared to those in CM[59] and the presence of more functionally active mitochondria in the TM in this study is in agreement with the earlier report.

While immunolocalization studies suggest that ANP/NPRA signaling would have a more direct effect on the TM cell gene expression program, our *in vitro* experiments cannot completely rule out similar effects of ANP on CM cells. This is because all metabolic and gene expression assays were performed on cells derived from the entire E11.5 ventricular myocardium without separating TM and CM cells. However, such cell separation studies are limited by the lack of well-established cell surface markers for TM and CM cells. As an alternative approach, ANP and Hey2-based reporter mouse models can be used to differentiate TM and CM cells respectively.[29] Indeed, previous work from our lab found that ANP+/lacZ + E11.5 ventricular cells fractionated from an ANF-lacZ reporter model[60] expressed higher levels of VCS markers (Cx40 and HCN4) compared to those in ANP-/lacZ-cells.[61] While such observations indicate differences in ANP-mediated gene expression effects in ANP+ (TM) vs. ANP- (CM) cells, completing comprehensive mechanistic *in vitro* experiments using such lineage tracking methods is technically challenging due to the requirement of pooling several hundreds of genotyped E11.5 ventricles for cell fractionation. Notably, correlations between histological findings and primary culture results presented in this study need further experimental validation using alternative methods of TM and CM cell fractionation in future studies. Based on the current literature, Cx40 and ANP are the only known markers for the primitive or developing VCS cells present in the E11.5 TM and subsequently Cx40 expression is known to be restricted to VCS cells at

E16.5 stage. While E16.5 VCS cells may be an appropriate model system to study the effects of ANP, these cells would be developmentally distinct from the primitive VCS cells found at E11.5 stage that were previously shown to be unresponsive to other VCS induction factors such as NRG-1.[7] Nevertheless, additional studies are required to determine the role of ANP in the proliferation and maturation of E16.5 as well as postnatal VCS cells.

Treatment of E11.5 ventricular cells with either ANP or fatty acids led to increased gene expression of PPARγ and Cx40. No PPARγ binding sequences have been identified in the published Cx40 5′-flanking and promoter regions.[62,63] Transcription factor mapping of a 150Kb mouse BAC clone (GenBank# AC115294.5) containing the published mouse Cx40 promoter region[63] revealed the presence of conserved sequences for one PPARγ responsive element[64] (between −26520 and −26507) and four Etv1 binding sites[65] (between −987 and −37746) in the mouse Cx40 5′ flanking region. Fatty acids are natural ligands for PPARγ and inhibition of PPARγ decreased Cx40 expression in response to exogenous ANP or fatty acid treatments. Co-treatment of cultures with both ANP and fatty acids showed an additive effect on lipid accumulation and Cx40 expression. Taken together, these results suggest that ANP and fatty acid treatments can promote VCS cell differentiation by super activating the PPARγ mediated effect on Cx40 expression levels. While conditional deletion of PPARγ was shown to cause membranous ventricular septal defects in the embryonic mouse hearts,[66] inducible deletion of PPARγ gene in cardiomyocytes of the adult mouse heart led to reduced levels of transcripts and proteins important for lipid uptake and metabolism (CD36, FABP, CPT1) as well as decreases in myocardial fatty acid utilization and contractility.[67] Earlier studies identified Cx40 as one of the upregulated transcripts in response to the activation of PPARγ in the placental extravillous cytotrophoblast cultures.[68] Additionally, PPARγ is also essential for the transcription of Irx3 gene which is known to regulate Cx40 expression and VCS formation.[69,70] In line with these previous reports, pharmacological inhibition of PPARγ in this study led to abrogation of ANP and fatty acid mediated increases in Cx40 expression.

PPARγ inhibitor (GW9662) significantly decreased Cx40 expression both in the presence or absence of ANP or OA + LA co-treatments. In previous studies, we showed that E11.5 ventricular cells can secrete the biologically active form of ANP.[28] Based on these observations, it is possible that reduction in Cx40 expression by GW9662 treatment alone in the absence of exogenous ANP could be due to inhibition of basal levels of PPARγ expression stimulated by the endogenous ANP in our experiments. Notably, when the same dose of GW9662 was administered without or with either ANP or OA + LA treatments, Cx40 expression was significantly higher in co-treatment groups compared to GW9662 treatment alone possibly due to the additive effects of both exogenous and endogenous ANP in these experiments. We previously reported that ANP treatment of embryonic ventricular cells decreased the gene expression of miR-27b and miR-133.[8] Importantly, these two microRNAs (miR-27b and miR-133) were also shown to decrease the expression of PPARγ in cardiomyocytes and other cell types.[8,71,72] Moreover, miR-27b expression was shown to be robust in the CM of E10.5 hearts[73] and it is possible that lower expression of miR-27b due to high levels of ANP may enhance PPARγ expression in the TM. Based on our *in vitro* findings, increased PPARγ expression in the embryonic TM is likely to promote lipid metabolism and VCS cell differentiation. Taken together, our data suggests that high levels of ANP expression in the TM decreases the expression of miR-27b and miR-133 and promotes the expression of PPARγ along with the VCS marker gene expression.

Several single gene mutations affecting FAO result in defective conduction system development.[19] In this study, inhibition of FAO using etomoxir decreased the expression of Cx40 and sarc. myosin levels in cultures treated with or without ANP. Given that Cx40 expression is tightly correlated with ANP signaling, intracellular lipid content and FAO in both cultured cells and E11.5 TM, metabolites of β-oxidation and TCA cycle are likely to play a mechanistic role in VCS marker gene expression. Excess acetyl CoA can escape to the cytoplasm from mitochondria using the citrate transport shuttle and is known to regulate gene expression via acetylation of histones and other proteins.[42] Significant increases in the expression levels of a histone acetyltransferase (MYST1) and acetylated histone H3 in ANP treated cultures support the notion that histone acetylation is important for ANP-mediated Cx40 expression. The transcription factor Etv1/ER81 regulates the expression of Cx40, Nkx2.5 and Scn5a and it is essential for VCS development.[74] Previous studies demonstrated that acetylation of Etv1 on lysine residues (K33 and K116) by two acetyltransferases p300 and P/CAF enhances its transactivation and DNA binding properties as well as half-life.[75] The Cx40 promoter is also regulated by the transcription factors Nkx2.5, GATA4 and Tbx5[76] and acetylation was shown to be important for their functions.[77–79] Overall, these reports offer a mechanistic explanation for ANP mediated protein acetylation in the regulation of Cx40 expression.

In conclusion, we showed that spatial expression patterns for ANP and NPRA overlapped with markers of VCS cells and lipid metabolism in the E11.5 TM. Primary culture studies indicated that ANP mediated intracellular lipid accumulation and metabolic changes in a subset of E11.5 ventricular cells promote $Cx40^{+}$ VCS cell proliferation and differentiation *in vitro*. Finally, our work proposes that acetylation of epigenetic regulators can be a potential mechanism in VCS cell differentiation.

Limitations of the study

Histological findings from E11.5 ventricles could be further substantiated by examining the effects of ANP/NPRA signaling on cellular metabolism and VCS marker gene expression in primary cultures derived from the fractionated TM and CM cells. While such compartment specific cell separation is technically challenging, this limitation is partly offset by confirming the stimulatory effects of ANP on FAO and VCS marker expression in primary cultures derived from E11.5 whole ventricles. We anticipate that this limitation could be addressed when reliable cell fractionation techniques become available. While ANP and Cx40 are the only known markers for the primitive VCS cells found at E11.5 stage, these markers are expressed in most TM cells at this stage. Findings in this study could have been further validated by using cells from later stages of heart development such as E16.5 wherein the Cx40 expression is restricted to VCS network. Follow-up validation studies using fractionated TM, CM, and VCS cells from additional developmental stages could further substantiate the importance of ANP/NPRA signaling in VCS cell proliferation and differentiation.

STAR★METHODS

Detailed methods are provided in the online version of this paper and include the following:

- KEY RESOURCES TABLE
- RESOURCE AVAILABILITY
  - Lead contact
  - Materials availability
  - Data and code availability
- EXPERIMENTAL MODEL AND STUDY PARTICIPANT DETAILS
  - Embryonic ventricular cell cultures
- METHOD DETAILS
  - Drug and fatty acid treatment protocols
  - Immune cytochemistry
  - Cell proliferation assays by click-iT Edu and pan-phospho-aurora kinase labeling
  - BODIPY staining for lipid droplets
  - Cell number quantification
  - Embryonic heart cross-sections and immunohistochemistry
  - In-cell westerns
  - Total RNA extraction and RT-qPCR
  - Protein extraction and western blotting
  - JC10 staining
  - Seahorse assay
  - Lipid extraction and Ultra-HPLC method for lipid analysis
  - High-resolution tandem mass spectrometry and lipidomics
- QUANTIFICATION AND STATISTICAL ANALYSIS
  - Data cleanup and statistical analysis of lipids
  - Statistical analysis

SUPPLEMENTAL INFORMATION

Supplemental information can be found online at https://doi.org/10.1016/j.isci.2023.108748.

ACKNOWLEDGMENTS

We thank Sarita Chinni (Pasumarthi Lab) and Dalhousie CORES for excellent technical assistance. This work was supported by grants from the Heart and Stroke Foundation of Canada (G-18-0022140 to KBSP), Faculty of Medicine, Dalhousie (R35225 to KBSP) and the Canadian Institutes of Health Research (to CRM). A.M. is supported by the Nova Scotia Graduate Scholarship, the Dalhousie Medical Research Foundation (DMRF) McDonald Scholarship and the DMRF Harry and Imogen Miller Graduate Scholarship.

AUTHOR CONTRIBUTIONS

A.M. and K.B.S.P. conceptualized the study. A.M. and M.T. performed the experiments and collected the datasets. A.M., M.T., S.S., and K.B.S.P. analyzed the data. K.B.S.P. provided overall research funding, ethics approval, critical data evaluation and project supervision. C.R.M. provided insights and funding for lipidomic studies. S.S. wrote the code and performed lipidomic data analysis. A.M. wrote the original manuscript draft and K.B.S.P. reviewed and edited the manuscript. All authors read and participated in editing and approval of the final manuscript.

DECLARATION OF INTERESTS

No conflicts of interest, financial or otherwise, are declared by the authors.

INCLUSION AND DIVERSITY

We support inclusive, diverse, and equitable conduct of research.

Received: May 15, 2023
Revised: September 15, 2023
Accepted: December 12, 2023
Published: December 14, 2023

REFERENCES

1. Choquet, C., Kelly, R.G., and Miquerol, L. (2020). Nkx2-5 defines distinct scaffold and recruitment phases during formation of the murine cardiac Purkinje fiber network. Nat. Commun. *11*, 5300.
2. McMullen, N.M., Zhang, F., Hotchkiss, A., Bretzner, F., Wilson, J.M., Ma, H., Wafa, K., Brownstone, R.M., and Pasumarthi, K.B.S. (2009). Functional characterization of cardiac progenitor cells and their derivatives in the embryonic heart post-chamber formation. Dev. Dyn. *238*, 2787–2799.
3. Lahiri, S.K., Hulsurkar, M.M., and Wehrens, X.H. (2021). Cellular regeneration as a potential strategy to treat cardiac conduction disorders. J. Clin. Invest. *131*, e152185.
4. Ideker, R.E., Kong, W., and Pogwizd, S. (2009). Purkinje fibers and arrhythmias. Pacing Clin. Electrophysiol. *32*, 283–285.
5. Gourdie, R.G., Wei, Y., Kim, D., Klatt, S.C., and Mikawa, T. (1998). Endothelin-induced conversion of embryonic heart muscle cells into impulse-conducting Purkinje fibers. Proc. Natl. Acad. Sci. USA *95*, 6815–6818.
6. van Weerd, J.H., and Christoffels, V.M. (2016). The formation and function of the cardiac conduction system. Development *143*, 197–210.
7. Rentschler, S., Zander, J., Meyers, K., France, D., Levine, R., Porter, G., Rivkees, S.A., Morley, G.E., and Fishman, G.I. (2002). Neuregulin-1 promotes formation of the murine cardiac conduction system. Proc. Natl. Acad. Sci. USA *99*, 10464–10469.
8. Govindapillai, A., Hotchkiss, A., Baguma-Nibasheka, M., Rose, R.A., Miquerol, L., Smithies, O., Maeda, N., and Pasumarthi, K.B.S. (2018). Characterizing the role of atrial natriuretic peptide signaling in the development of embryonic ventricular conduction system. Sci. Rep. *8*, 6939.
9. Goodyer, W.R., and Wu, S.M. (2018). Fates Aligned: Origins and Mechanisms of Ventricular Conduction System and Ventricular Wall Development. Pediatr. Cardiol. *39*, 1090–1098.
10. Houweling, A.C., van Borren, M.M., Moorman, A.F.M., and Christoffels, V.M. (2005). Expression and regulation of the atrial natriuretic factor encoding gene Nppa during development and disease. Cardiovasc. Res. *67*, 583–593.
11. Anand-Srivastava, M.B., Thibault, G., Sola, C., Fon, E., Ballak, M., Charbonneau, C., Haile-Meskel, H., Garcia, R., Genest, J., and Cantin, M. (1989). Atrial natriuretic factor in Purkinje fibers of rabbit heart. Hypertension *13*, 789–798.
12. Cantin, M., Thibault, G., Haile-Meskel, H., Ding, J., Milne, R.W., Ballak, M., Charbonneau, C., Nemer, M., Drouin, J., Garcia, R., et al. (1989). Atrial natriuretic factor in the impulse-conduction system of rat cardiac ventricles. Cell Tissue Res. *256*, 309–325.
13. Moorman, A.F., de Jong, F., Denyn, M.M., and Lamers, W.H. (1998). Development of the cardiac conduction system. Circ. Res. *82*, 629–644.
14. Delorme, B., Dahl, E., Jarry-Guichard, T., Marics, I., Briand, J.P., Willecke, K., Gros, D., and Théveniau-Ruissy, M. (1995). Developmental regulation of connexin 40 gene expression in mouse heart correlates with the differentiation of the conduction system. Dev. Dyn. *204*, 358–371.
15. Sedmera, D., Reckova, M., DeAlmeida, A., Coppen, S.R., Kubalak, S.W., Gourdie, R.G., and Thompson, R.P. (2003). Spatiotemporal pattern of commitment to slowed proliferation in the embryonic mouse heart indicates progressive differentiation of the cardiac conduction system. Anat. Rec. A Discov. Mol. Cell. Evol. Biol. *274*, 773–777.
16. Pasumarthi, K.B.S., and Field, L.J. (2002). Cardiomyocyte cell cycle regulation. Circ. Res. *90*, 1044–1054.
17. Morita, Y., and Tohyama, S. (2020). Metabolic Regulation of Cardiac Differentiation and Maturation in Pluripotent Stem Cells: A Lesson from Heart Development. JMA J. *3*, 193–200.
18. Yang, X., Rodriguez, M.L., Leonard, A., Sun, L., Fischer, K.A., Wang, Y., Ritterhoff, J., Zhao, L., Kolwicz, S.C., Pabon, L., et al. (2019). Fatty Acids Enhance the Maturation of Cardiomyocytes Derived from Human Pluripotent Stem Cells. Stem Cell Rep. *13*, 657–668.
19. Bonnet, D., Martin, D., De Lonlay, P., Villain, E., Jouvet, P., Rabier, D., Brivet, M., and Saudubray, J.M. (1999). Arrhythmias and conduction defects as presenting symptoms of fatty acid oxidation disorders in children. Circulation *100*, 2248–2253.
20. Ji, S., You, Y., Kerner, J., Hoppel, C.L., Schoeb, T.R., Chick, W.S.H., Hamm, D.A., Sharer, J.D., and Wood, P.A. (2008). Homozygous carnitine palmitoyltransferase 1b (muscle isoform) deficiency is lethal in the mouse. Mol. Genet. Metab. *93*, 314–322.
21. Cai, K., Wang, F., Lu, J.Q., Shen, A.N., Zhao, S.M., Zang, W.D., Gui, Y.H., and Zhao, J.Y. (2022). Nicotinamide Mononucleotide Alleviates Cardiomyopathy Phenotypes Caused by Short-Chain Enoyl-Coa Hydratase 1 Deficiency. JACC. Basic Transl. Sci. *7*, 348–362.
22. Barak, Y., Liao, D., He, W., Ong, E.S., Nelson, M.C., Olefsky, J.M., Boland, R., and Evans, R.M. (2002). Effects of peroxisome proliferator-activated receptor delta on placentation, adiposity, and colorectal cancer. Proc. Natl. Acad. Sci. USA *99*, 303–308.
23. Barak, Y., Nelson, M.C., Ong, E.S., Jones, Y.Z., Ruiz-Lozano, P., Chien, K.R., Koder, A., and Evans, R.M. (1999). PPAR gamma is required for placental, cardiac, and adipose tissue development. Mol. Cell *4*, 585–595.
24. Jordan, J., Birkenfeld, A.L., Melander, O., and Moro, C. (2018). Natriuretic Peptides in Cardiovascular and Metabolic Crosstalk: Implications for Hypertension Management. Hypertension *72*, 270–276.
25. Zois, N.E., Bartels, E.D., Hunter, I., Kousholt, B.S., Olsen, L.H., and Goetze, J.P. (2014). Natriuretic peptides in cardiometabolic regulation and disease. Nat. Rev. Cardiol. *11*, 403–412.
26. Suffee, N., Moore-Morris, T., Farahmand, P., Rücker-Martin, C., Dilanian, G., Fradet, M., Sawaki, D., Derumeaux, G., LePrince, P., Clément, K., et al. (2017). Atrial natriuretic peptide regulates adipose tissue accumulation in adult atria. Proc. Natl. Acad. Sci. USA *114*, E771–E780.
27. Ramosaj, M., Madsen, S., Maillard, V., Scandella, V., Sudria-Lopez, D., Yuizumi, N., Telley, L., and Knobloch, M. (2021). Lipid droplet availability affects neural stem/progenitor cell metabolism and proliferation. Nat. Commun. *12*, 7362.
28. Hotchkiss, A., Feridooni, T., Baguma-Nibasheka, M., McNeil, K., Chinni, S., and Pasumarthi, K.B.S. (2015). Atrial natriuretic peptide inhibits cell cycle activity of embryonic cardiac progenitor cells via its NPRA receptor signaling axis. Am. J. Physiol. Cell Physiol. *308*, C557–C569.
29. Tian, X., Li, Y., He, L., Zhang, H., Huang, X., Liu, Q., Pu, W., Zhang, L., Li, Y., Zhao, H., et al. (2017). Identification of a hybrid myocardial zone in the mammalian heart after birth. Nat. Commun. *8*, 87.
30. Carper, D., Coué, M., Nascimento, E.B.M., Barquissau, V., Lagarde, D., Pestourie, C., Laurens, C., Petit, J.V., Soty, M., Monbrun, L., et al. (2020). Atrial Natriuretic Peptide Orchestrates a Coordinated Physiological Response to Fuel Non-shivering Thermogenesis. Cell Rep. *32*, 108075.
31. Cardoso, A.C., Lam, N.T., Savla, J.J., Nakada, Y., Pereira, A.H.M., Elnwasany, A., Menendez-Montes, I., Ensley, E.L., Petric, U.B., Sharma, G., et al. (2020). Mitochondrial Substrate Utilization Regulates Cardiomyocyte Cell Cycle Progression. Nat. Metab. *2*, 167–178.
32. Sharpe, A.J., and McKenzie, M. (2018). Mitochondrial Fatty Acid Oxidation Disorders Associated with Short-Chain Enoyl-CoA Hydratase (ECHS1) Deficiency. Cells *7*.
33. Younes, N., Alsahan, B.S., Al-Mesaifri, A.J., Da'as, S.I., Pintus, G., Majdalawieh, A.F., and Nasrallah, G.K. (2022). JC-10 probe as a novel method for analyzing the mitochondrial membrane potential and cell stress in whole zebrafish embryos. Toxicol. Res. *11*, 77–87.
34. Garner, D.L., Thomas, C.A., Joerg, H.W., DeJarnette, J.M., and Marshall, C.E. (1997). Fluorometric assessments of mitochondrial function and viability in cryopreserved bovine spermatozoa. Biol. Reprod. *57*, 1401–1406.
35. Piquereau, J., and Ventura-Clapier, R. (2018). Maturation of Cardiac Energy Metabolism During Perinatal Development. Front. Physiol. *9*, 959.
36. Tavasoli, M., Feridooni, T., Feridooni, H., Sokolenko, S., Mishra, A., Lefsay, A., Srinivassane, S., Reid, S.A., Rowsell, J., Praest, M., et al. (2022). A mouse model of inherited choline kinase β-deficiency presents with specific cardiac abnormalities and a predisposition to arrhythmia. J. Biol. Chem. *298*, 101716.
37. Warshaw, J.B. (1972). Cellular energy metabolism during fetal development. IV. Fatty acid activation, acyl transfer and fatty acid oxidation during development of the chick and rat. Dev. Biol. *28*, 537–544.
38. Makinde, A.O., Kantor, P.F., and Lopaschuk, G.D. (1998). Maturation of fatty acid and carbohydrate metabolism in the newborn heart. Mol. Cell. Biochem. *188*, 49–56.
39. Warshaw, J.B., and Terry, M.L. (1970). Cellular energy metabolism during fetal development. II. Fatty acid oxidation by the developing heart. J. Cell Biol. *44*, 354–360.
40. Jiang, P., Du, W., and Wu, M. (2014). Regulation of the pentose phosphate pathway in cancer. Protein Cell *5*, 592–602.
41. Patel, J.H., Ong, D.J., Williams, C.R., Callies, L.K., and Wills, A.E. (2022). Elevated pentose phosphate pathway flux supports appendage regeneration. Cell Rep. *41*, 111552.
42. Sivanand, S., Viney, I., and Wellen, K.E. (2018). Spatiotemporal Control of Acetyl-CoA Metabolism in Chromatin Regulation. Trends Biochem. Sci. *43*, 61–74.

43. Cao, T., Liccardo, D., LaCanna, R., Zhang, X., Lu, R., Finck, B.N., Leigh, T., Chen, X., Drosatos, K., and Tian, Y. (2019). Fatty Acid Oxidation Promotes Cardiomyocyte Proliferation Rate but Does Not Change Cardiomyocyte Number in Infant Mice. Front. Cell Dev. Biol. *7*, 42.
44. Denis, J.F., Diagbouga, M.R., Molica, F., Hautefort, A., Linnerz, T., Watanabe, M., Lemeille, S., Bertrand, J.Y., and Kwak, B.R. (2019). KLF4-Induced Connexin40 Expression Contributes to Arterial Endothelial Quiescence. Front. Physiol. *10*, 80.
45. Balogh, S., Naus, C.C., and Merrifield, P.A. (1993). Expression of gap junctions in cultured rat L6 cells during myogenesis. Dev. Biol. *155*, 351–360.
46. Yeganeh, A., Stelmack, G.L., Fandrich, R.R., Halayko, A.J., Kardami, E., and Zahradka, P. (2012). Connexin 43 phosphorylation and degradation are required for adipogenesis. Biochim. Biophys. Acta *1823*, 1731–1744.
47. Gerhart, S.V., Eble, D.M., Burger, R.M., Oline, S.N., Vacaru, A., Sadler, K.C., Jefferis, R., and Iovine, M.K. (2012). The Cx43-like connexin protein Cx40.8 is differentially localized during fin ontogeny and fin regeneration. PLoS One *7*, e31364.
48. Haggarty, P. (2010). Fatty acid supply to the human fetus. Annu. Rev. Nutr. *30*, 237–255.
49. Lafontan, M., Moro, C., Sengenes, C., Galitzky, J., Crampes, F., and Berlan, M. (2005). An unsuspected metabolic role for atrial natriuretic peptides: the control of lipolysis, lipid mobilization, and systemic nonesterified fatty acids levels in humans. Arterioscler. Thromb. Vasc. Biol. *25*, 2032–2042.d8.
50. Delporte, C., Winand, J., Poloczek, P., Von Geldern, T., and Christophe, J. (1992). Discovery of a potent atrial natriuretic peptide antagonist for ANPA receptors in the human neuroblastoma NB-OK-1 cell line. Eur. J. Pharmacol. *224*, 183–188.
51. Heisler, S. (1989). Direct binding of atrial natriuretic factor to adrenocortical mitochondria. Eur. J. Pharmacol. *162*, 281–288.
52. Morel, G., Mesguich, P., Chabot, J.G., Belles-Isles, M., Jeandel, L., and Heisler, S. (1989). Internalization of atrial natriuretic peptide by adrenal glomerulosa cells. Biol. Cell *65*, 181–188.
53. Solmonson, A., Faubert, B., Gu, W., Rao, A., Cowdin, M.A., Menendez-Montes, I., Kelekar, S., Rogers, T.J., Pan, C., Guevara, G., et al. (2022). Compartmentalized metabolism supports midgestation mammalian development. Nature *604*, 349–353.
54. Beutner, G., Eliseev, R.A., and Porter, G.A. (2014). Initiation of electron transport chain activity in the embryonic heart coincides with the activation of mitochondrial complex 1 and the formation of supercomplexes. PLoS One *9*, e113330.
55. Sosa, V., Carbó, R., and Guarner, V. (2007). Participation of glucose transporters on atrial natriuretic peptide-induced glucose uptake by adult and neonatal cardiomyocytes under oxygenation and hypoxia. Eur. J. Pharmacol. *568*, 83–88.
56. Coué, M., Barquissau, V., Morigny, P., Louche, K., Lefort, C., Mairal, A., Carpéné, C., Viguerie, N., Arner, P., Langin, D., et al. (2018). Natriuretic peptides promote glucose uptake in a cGMP-dependent manner in human adipocytes. Sci. Rep. *8*, 1097.
57. Llurba Olive, E., Xiao, E., Natale, D.R., and Fisher, S.A. (2018). Oxygen and lack of oxygen in fetal and placental development, feto-placental coupling, and congenital heart defects. Birth Defects Res. *110*, 1517–1530.
58. Guimarães-Camboa, N., Stowe, J., Aneas, I., Sakabe, N., Cattaneo, P., Henderson, L., Kilberg, M.S., Johnson, R.S., Chen, J., McCulloch, A.D., et al. (2015). HIF1α Represses Cell Stress Pathways to Allow Proliferation of Hypoxic Fetal Cardiomyocytes. Dev. Cell *33*, 507–521.
59. Menendez-Montes, I., Escobar, B., Palacios, B., Gómez, M.J., Izquierdo-Garcia, J.L., Flores, L., Jiménez-Borreguero, L.J., Aragones, J., Ruiz-Cabello, J., Torres, M., and Martin-Puig, S. (2016). Myocardial VHL-HIF Signaling Controls an Embryonic Metabolic Switch Essential for Cardiac Maturation. Dev. Cell *39*, 724–739.
60. Habets, P.E.M.H., Moorman, A.F.M., Clout, D.E.W., van Roon, M.A., Lingbeek, M., van Lohuizen, M., Campione, M., and Christoffels, V.M. (2002). Cooperative action of Tbx2 and Nkx2.5 inhibits ANF expression in the atrioventricular canal: implications for cardiac chamber formation. Genes Dev. *16*, 1234–1246.
61. Hotchkiss, A. (2013). The Effects of Calcium Channel Blockade and Atrial Natriuretic Peptide Signalling on Proliferation and Differentiation of Cardiac Progenitor Cells (Dalhousie University).
62. Dupays, L., Mazurais, D., Rücker-Martin, C., Calmels, T., Bernot, D., Cronier, L., Malassiné, A., Gros, D., and Théveniau-Ruissy, M. (2003). Genomic organization and alternative transcripts of the human Connexin40 gene. Gene *305*, 79–90.
63. Seul, K.H., Tadros, P.N., and Beyer, E.C. (1997). Mouse connexin40: gene structure and promoter analysis. Genomics *46*, 120–126.
64. Juge-Aubry, C., Pernin, A., Favez, T., Burger, A.G., Wahli, W., Meier, C.A., and Desvergne, B. (1997). DNA binding properties of peroxisome proliferator-activated receptor subtypes on various natural peroxisome proliferator response elements. Importance of the 5'-flanking region. J. Biol. Chem. *272*, 25252–25259.
65. Cooper, C.D.O., Newman, J.A., Aitkenhead, H., Allerston, C.K., and Gileadi, O. (2015). Structures of the Ets Protein DNA-binding Domains of Transcription Factors Etv1, Etv4, Etv5, and Fev: DETERMINANTS OF DNA BINDING AND REDOX REGULATION BY DISULFIDE BOND FORMATION. J. Biol. Chem. *290*, 13692–13709.
66. Zhou, L., Wang, Z.Z., Xiao, Z.C., and Tu, L. (2020). Effects of PPAR-γ in the Myocardium on the Development of Ventricular Septation. Curr. Med. Sci. *40*, 313–319.
67. Luo, J., Wu, S., Liu, J., Li, Y., Yang, H., Kim, T., Zhelyabovska, O., Ding, G., Zhou, Y., Yang, Y., and Yang, Q. (2010). Conditional PPARγ knockout from cardiomyocytes of adult mice impairs myocardial fatty acid utilization and cardiac function. Am. J. Transl. Res. *3*, 61–72.
68. Segond, N., Degrelle, S.A., Berndt, S., Clouqueur, E., Rouault, C., Saubamea, B., Dessen, P., Fong, K.S.K., Csiszar, K., Badet, J., et al. (2013). Transcriptome analysis of PPARγ target genes reveals the involvement of lysyl oxidase in human placental cytotrophoblast invasion. PLoS One *8*, e79413.
69. Wei, D., Raza, S.H.A., Zhang, J., Wang, X., Khan, R., Ma, Y., Zhang, G., Luoreng, Z., and Zan, L. (2020). Characterization of the promoter region of the bovine. Physiol. Genom. *52*, 160–167.
70. Zhang, S.S., Kim, K.H., Rosen, A., Smyth, J.W., Sakuma, R., Delgado-Olguín, P., Davis, M., Chi, N.C., Puviindran, V., Gaborit, N., et al. (2011). Iroquois homeobox gene 3 establishes fast conduction in the cardiac His-Purkinje network. Proc. Natl. Acad. Sci. USA *108*, 13576–13581.
71. Lee, J.J., Drakaki, A., Iliopoulos, D., and Struhl, K. (2012). MiR-27b targets PPARγ to inhibit growth, tumor progression and the inflammatory response in neuroblastoma cells. Oncogene *31*, 3818–3825.
72. Portius, D., Sobolewski, C., and Foti, M. (2017). MicroRNAs-Dependent Regulation of PPARs in Metabolic Diseases and Cancers. PPAR Res. *2017*, 7058424.
73. Chinchilla, A., Lozano, E., Daimi, H., Esteban, F.J., Crist, C., Aranega, A.E., and Franco, D. (2011). MicroRNA profiling during mouse ventricular maturation: a role for miR-27 modulating Mef2c expression. Cardiovasc. Res. *89*, 98–108.
74. Shekhar, A., Lin, X., Liu, F.Y., Zhang, J., Mo, H., Bastarache, L., Denny, J.C., Cox, N.J., Delmar, M., Roden, D.M., et al. (2016). Transcription factor ETV1 is essential for rapid conduction in the heart. J. Clin. Invest. *126*, 4444–4459.
75. Goel, A., and Janknecht, R. (2003). Acetylation-mediated transcriptional activation of the ETS protein ER81 by p300, P/CAF, and HER2/Neu. Mol. Cell Biol. *23*, 6243–6254.
76. Linhares, V.L.F., Almeida, N.A.S., Menezes, D.C., Elliott, D.A., Lai, D., Beyer, E.C., Campos de Carvalho, A.C., and Costa, M.W. (2004). Transcriptional regulation of the murine Connexin40 promoter by cardiac factors Nkx2-5, GATA4 and Tbx5. Cardiovasc. Res. *64*, 402–411.
77. Tang, X., Ma, H., Han, L., Zheng, W., Lu, Y.B., Chen, X.F., Liang, S.T., Wei, G.H., Zhang, Z.Q., Chen, H.Z., and Liu, D.P. (2016). SIRT1 deacetylates the cardiac transcription factor Nkx2.5 and inhibits its transcriptional activity. Sci. Rep. *6*, 36576.
78. Kawamura, T., Ono, K., Morimoto, T., Wada, H., Hirai, M., Hidaka, K., Morisaki, T., Heike, T., Nakahata, T., Kita, T., and Hasegawa, K. (2005). Acetylation of GATA-4 is involved in the differentiation of embryonic stem cells into cardiac myocytes. J. Biol. Chem. *280*, 19682–19688.
79. Ghosh, T.K., Aparicio-Sánchez, J.J., Buxton, S., Ketley, A., Mohamed, T., Rutland, C.S., Loughna, S., and Brook, J.D. (2018). Acetylation of TBX5 by KAT2B and KAT2A regulates heart and limb development. J. Mol. Cell. Cardiol. *114*, 185–198.
80. Tavasoli, M., Lahire, S., Sokolenko, S., Novorolsky, R., Reid, S.A., Lefsay, A., Otley, M.O.C., Uaesoontrachoon, K., Rowsell, J., Srinivassane, S., et al. (2022). Mechanism of action and therapeutic route for a muscular dystrophy caused by a genetic defect in lipid metabolism. Nat. Commun. *13*, 1559.

STAR★METHODS

KEY RESOURCES TABLE

REAGENT or RESOURCE	SOURCE	IDENTIFIER
Antibodies		
Connexin 40 (Cx40)	Alpha Diagnostic International	Cat# Cx40-A; RRID: AB_1616128
Sarcomeric myosin heavy chain (Sarc. MHC)	Developmental Studies Hybridoma Bank, Iowa	Cat#MF20; RRID: AB_2147781
Anti-acetyl-histone H3	Millipore Sigma	Cat#06-911; RRID: AB_310294
Anti-HCN4 antibody	Alomone Lab	Cat# APC-052; RRID: AB_2039906
Anti- ANP antibody	Millipore Sigma	Cat# CBL66; RRID: AB_2283096
Rabbit Polyclonal PGCA antibody	FabGennix	Cat#PGCA-101AP; RRID: AB_2315119
Phopshorylated pyruvate dehydrogense (p-PDH) antibody	Cell Signaling Technology	Cat# 37115S; RRID: AB_2923272
Enoyl CoA hydratse (ECHS1)	Developmental Studies Hybridoma Bank, Iowa	Cat#AFFN-ECHS1-5F7; RRID: AB_2617542
Pan-phospho-aurora kinase antibodies (Phospho-aurora A (Thr288)/aurora B (Thr232)/aurora C (Thr198) (D13A11) XP Rabbit polyclonal antibody	Cell Signaling Technology	Cat#2914; RRID: AB_2061631
Secondary goat anti-mouse antibody conjugated to Alexa Fluor 488	Thermo Fisher	Cat#A11017; RRID: AB_2534084
Secondary goat anti-mouse antibody conjugated to Alexa Fluor 555	Thermo Fisher	Cat#A21425; RRID: AB_1500751
Secondary goat anti-rabbit antibody conjugated to Alexa Fluor 555	Thermo Fisher	Cat#A21430; RRID: AB_10374475
Secondary goat anti-rabbit antibody conjugated to Alexa Fluor 488	Thermo Fisher	Cat#A11070; RRID: AB_2534114
Secondary goat anti-rabbit antibody conjugated to Alexa Fluor 647	Cell Signaling Technology	Cat#4414; RRID: AB_10693544
Anti-rabbit IgG (H+L) DyLight 800 PEG conjugate	New England Biolabs	Cat#5151P; RRID: AB_10697505
anti-mouse IgG (H+L) DyLight 680 conjugate	New England Biolabs	Cat#5470P; RRID: AB_10696895
Chemicals, peptides, and recombinant proteins		
Hoechst 33258	Millipore Sigma	Cat#14530
1x antibiotic/antimycotic	Thermo Fisher	Cat#15240-062
type I collagenase	Worthington Biochemical Corp	Cat#LS004196
Dulbecco's Modified Eagles Medium (DMEM)	Wisent	Cat#319-005-CL
DMEM base medium	Agilent	Cat#103575-100
Fetal bovine serum	Millipore Sigma	Cat#F1051
Atrial Natriuretic Peptide	Bachem	Cat#: H-2100
A71915	Bachem	Cat#: H-3048
GW9662	Millipore Sigma	Cat#M6191
Etomoxir	Millipore Sigma	Cat#E1905
Oleic Acid-Albumin from bovine serum	Millipore Sigma	Cat#O3008

(*Continued on next page*)

Continued

REAGENT or RESOURCE	SOURCE	IDENTIFIER
Linoleic Acid-Albumin from bovine serum albumin	Millipore Sigma	Cat#L9530
Bovine Serum Albumin powder	Thermo Fisher	Cat#SH30574.02
Bovine Serum Albumin	Millipore Sigma	Cat# A1595
Goat serum	Thermo Fisher	Cat# 16210064
BODIPY 493/503	Thermo Fisher	Cat# D3922
Oligomycin	Focus Biomolecule	Cat#10-2092
Carbonyl cyanide-p-trifluoromethoxyphenylhydrazone (FCCP)	Millipore Sigma	Cat#C2920
Rotenone	Millipore Sigma	Cat#45656
Antimycin A	Millipore Sigma	Cat#A8674
Critical commercial assays		
Aurum™ Total RNA Mini	Biorad	Cat#732-6820
SuperScript VILO	Thermo Fisher	Cat#18090010
JC-10 Mitochondrial Membrane Potential Assay	AAT Bioquest	Cat#22204
Experimental models: Organisms/strains		
E11.5 timed pregnant CD1 mice	Charles River Laboratories, Senneville, Quebec	Cat#022
Oligonucleotides		
Primers for RT-qPCR, see Table S1	This Paper	N/A
Software and algorithms		
ImageJ	National Institutes of Health	https://imagej.nih.gov/ij/
Prism-GraphPad	Dotmatics	https://www.graphpad.com/scientific- software/prism/
Depsited data		
Custom code and raw data for lipidomic analysis	Zenodo https://zenodo.org/records/10290509	https://zenodo.org/badge/DOI/10.5281/zenodo.10290509.svg

RESOURCE AVAILABILITY

Lead contact

Further information and requests for resources and reagents should be directed to and will be fulfilled by the lead contact, Kishore Pasumarthi (kpasumar@dal.ca).

Materials availability

This study did not generate new unique reagents.

Data and code availability

- All data generated or analyzed in this study are included in this publication. All relevant data are available from the lead contact upon reasonable request.
- The custom code used for lipidomic analysis in this study has been submitted at Zenodo and is publicly available as of the date of publication. The DOI (https://zenodo.org/records/10290509) is also listed in the key resources table. Download all raw data files of lipidomic analysis into same file and run analysis.R to reproduce analysis plots from this study.
- Any additional information required to reanalyze the data reported in this paper is available from the lead contact upon reasonable request.

EXPERIMENTAL MODEL AND STUDY PARTICIPANT DETAILS

Embryonic ventricular cell cultures

E11.5 days timed-pregnant CD1 mice (Charles River Laboratories, Senneville, Quebec) were sacrificed in a 4% isoflurane-induced anesthetized state. Embryos were taken out from the uterine horns and kept in dishes containing warm PBS with 1x antibiotic/antimycotic (1x Ab/Am; Gibco, Thermofisher, Cat#15240-062) for further dissection. The whole embryonic hearts were removed, and the atria and outflow tracts were dissected out under the Leica MZ16F stereomicroscope (Leica Microsystems, Richmond Hill, Ontario, Canada). Only embryonic cardiac ventricles were pooled and placed in 0.2% v/v type I collagenase (Worthington Biochemical Corp., Cat#LS004196) in 1xPBS for ventricular tissue digestion at 37°C for 45 minutes on a rocking platform. After 45 minutes of incubation, the tissue was mechanically dissociated by trituration using a 200μL pipette tip. Then digested and dissociated tissue fragments were allowed to settle for 5 minutes for gravity separation of fibrous debris of embryonic ventricular tissue. The supernatant cell suspension was collected leaving debris in the tube and centrifuged at 1600 rcf (Eppendorf centrifuge, model#5415D) for 4 minutes at 4°C. Cell pellet formed after centrifugation was collected and washed twice with DMEM (Dulbecco's Modified Eagles Medium; Wisent, Cat#319-005-CL) containing 10% fetal bovine serum (FBS; Millipore Sigma, Cat#F1051) and 1x Ab/Am). Finally, cells were resuspended in 1 ml of 10% FBS-DMEM and cell number was determined using a hemocytometer. The cell suspension was resuspended in culture media to achieve desired cell density. Cells were plated on the fibronectin-coated 8-chambered slides (125,000 cells/well, Nunc, Rochester, New York, USA) for immunocytochemistry, or black-walled clear bottom 96- well plates (50,000 cells/well, Greiner Bio-One, North Carolina, USA) for in-cell western, or 35mm culture dishes (1,000,000 cells/dish, Falcon, Corning Inc, Cat#353001) for RNA and protein extraction, or 24-well Seahorse XF24 plates (40,000 cells/well, Agilent Tecnologies, Cat#100777-004) for seahorse assays. Cultures were incubated in a humid incubator at 37°C and 5% CO2 overnight before proceeding further drug/fatty acid treatment.

METHOD DETAILS

Drug and fatty acid treatment protocols

1μg/μL stock solution of ANP (Bachem, King of Prussia, Pennsylvania, USA Cat#: H- 2100) was prepared by dissolving 375μg of the compound in 375μL of sterile water (Ambion, USA). NPRA antagonist A71915 (Bachem, Cat#H-3048) stock solution was made by dissolving 0.5mg of the compound in 0.5mL of sterile water. PPARγ inhibitor GW9662 (MilliporeSigma, Cat#M6191) was prepared as an 18mM stock solution by dissolving 5mg of the compound in 1mL of DMSO. 10mM stock solution of etomoxir (MilliporeSigma, Cat#E1905) was prepared by adding 1.47mL of sterile water to 5mg of the compound.

The plated embryonic ventricular cells were maintained in a 10% FBS-DMEM medium overnight before the start of any treatment. Cell cultures were treated with different pharmacological agents every 24 hours over the experimental duration (1-3 days). The final concentration of drugs in cell culture were ANP: 0.3μM, A71915: 1μM, GW9662: 0.5μM, and etomoxir: 2.5μM. Control cultures were treated with the appropriate vehicle (H2O or DMSO) to match the condition of the drug-treated groups.

For experiments with fatty acids, cell culture media was supplemented with Oleic acid and Linoleic acid fatty acids conjugated with bovine serum albumin (MilliporeSigma, OA; Cat#O3008, LA; Cat#L9530). Two different concentrations of fatty acids (200μM and 400 μM) were supplemented in experiments with individual fatty acid treatments. Control cultures were supplemented with 200μM bovine serum albumin (BSA, MilliporeSigma, Cat#A1595). In experiments with fatty acid cocktail, cell culture was supplemented with 200μM of oleic acid and 200μM of linoleic acid, and to match the condition, control was supplemented with 400μM BSA. Cell cultures were maintained for three days before immunocytochemistry, In-cell Westerns, and protein extractions. The duration of treatment was 24 h in experiments for RNA extraction and seahorse assays and cell proliferation assays.

Immune cytochemistry

Following three days of cell culture, embryonic ventricular cell cultures were fixed with 4% paraformaldehyde w/v for 15 minutes at room temperature. Then cells were permeabilized in 0.1% Triton X-100 for 6 minutes. Subsequently, cells were washed twice with PBS, and were blocked using the blocking buffer solution (10% v/v goat serum (Thermofisher, Cat#16210064), and 1% w/v bovine serum albumin (BSA; Thermo Fisher, Cat#SH30574.02) in PBS) for one hour at room temperature. The blocking of cells was followed by addition of primary antibodies of interest to the cells in fresh blocking buffer solution for overnight incubation at 4°C. Connexin 40 (Cx40)/Gap junction alpha-5 Protein (CXA-5) antibody (Alpha Diagnostic International, Cat# Cx40-A) was used at 1:150 dilution (6.67μg/ml), Sarcomeric myosin antibody (Developmental Studies Hybridoma Bank, Iowa, Cat#MF20) was used at 1:150 dilution (0.15μg/ml) and anti-acetyl-histone H3 (Lys14; MilliporeSigma, Cat#06-911) was used at 1:75 dilution (13.3μg/ml). Next, cells were washed with PBS thrice for 5 minutes each and incubated with secondary antibodies in blocking buffer solution for 1 hour at room temperature. Secondary goat anti-mouse antibody conjugated to Alexa Fluor 488 (or 555) (1:150, Thermo Fisher) and goat anti-rabbit antibody conjugated to Alexa Fluor 555 (or 488) (1:150, Thermo Fisher) were used. Nuclei were stained with 0.5μg/ml Hoechst 33258 (MilliporeSigma, Cat#14530) in PBS for 3 minutes at room temperature. Further cells were washed with PBS twice and mounting medium 0.1% propyl gallate (Sigma) solution [0.1% w/v propyl gallate, 50% v/v glycerol (Thermo Fisher Scientific), 50% v/v PBS]. was spread before the coverslip was placed. Immuno-stained cells were examined using a Leica DM2500 microscope and images were captured using a Leica DFC 500 digital acquisition system.

Cell proliferation assays by click-iT Edu and pan-phospho-aurora kinase labeling

For analysis of VCS cells undergoing DNA synthesis, E11.5 ventricular cells were seeded on 8-chamber slides (125,000 cells/well) and 1 μl of Click-iT Edu stock solution (ThermoFisher Scientific, Cat#:44C10340) was added per chamber. Cells were also treated simultaneously with or without ANP and or A71915 as described in drug treatment protocol for 24 hours at 37°C. Prior to the staining, cells were washed twice with PBS for 2-minute. After PBS rinses, chamber slides were fixed with 4% w/v paraformaldehyde for 15 minutes at room temperature and then washed again twice with PBS for 2-minute. After fixation and PBS rinses, the chamber slides were then used for click-iT Edu labeling and immunofluorescence analysis of Cx40 and Sarc. MHC markers to track VCS cells. Immunocytochemistry was performed as described earlier. The Click-iT EdU assay was performed just after the incubation with secondary antibodies and prior to the Hoechst nuclear staining. Click-iT Plus EdU Alexa Fluor 647 Imaging Kit (ThermoFisher Scientific; Cat#: 10640) was used to assess cells undergoing DNA synthesis, and reagents from the kit were used to make a reaction cocktail as directed. A reaction cocktail was made with 10x Click-iT EdU buffer (88 μl), copper protectant (20 μl), Alexa Flour picoyl azide (2.5 μl), 10 X Reaction buffer (10 μl) and Nuclease free H2O (880 μl). After the PBS rinses, 200 μl of the reaction cocktail was added per well of the chamber slide and left to incubate in the dark for 30 minutes at room temperature. After 30 minutes, slides were rinsed twice with PBS for 2 minutes each, and Hoechst nuclear staining was performed. The slides were mounted with 0.1% propyl gallate and examined using the Leica DM2500 fluorescence microscope using appropriate excitation and emission filters and images were then captured using a Leica DFC 500 digital acquisition system.

For monitoring VCS cell proliferation, cultures were processed exactly as described for the DNA synthesis analysis, except Edu was not added to the culture medium. Proliferating VCS cells (Cx40+/sarc. MHC+) and Cx40 negative cardiomyoyctes (Cx40-/sarc. MHC+) were identified by co-staining with antibodies for Cx40, sarc. MHC and pan-phospho-aurora kinase (Cell Signaling Technology, Cat#2914, 1:100 dilution) and signals were visualized by secondary antibodies conjugated to Alexa Fluor 647, 555 and 488 respectively as described earlier. Mitotic events were further confirmed by Hoechst nuclear staining.

BODIPY staining for lipid droplets

BODIPY staining was performed after other immunostaining procedures (if any) were completed and before the mounting medium was spread. Cells were incubated with BODIPY 493/503 dye at 1:2000 dilution (0.5μg/ml) for 20 minutes at room temperature, to stain lipid droplets in the cells. Cells were then washed 3 times with PBS, each for 7 minutes, and mounted using 0.1% propyl gallate (Milliporesigma, cat#P-3130) solution [0.1% w/v propyl gallate and 50% v/v glycerol (Thermo Fisher Scientific) in PBS]. Stained cells were examined for lipid droplets using the Leica DM2500 fluorescence microscope using excitation filter and images were captured. BOPDIPY staining of cell cultures in a 96-well plate also followed the described procedure. BODIPY intensity was measured using POLARstar Omega microplate reader. The BODIPY intensity of each well was normalized by Hoescht intensity (DNA Content) before the analysis.

Cell number quantification

After immunostaining/ BODIPY/ click-iT EdU staining of E11.5 ventricular cell cultures, cell counting was performed through images captured using a Leica DFC 500 digital acquisition system. Images of cells from 10 random fields were taken per well/ treatment. Cell count was performed in blinded fashion from each group to avoid any observer's bias. The number of Hoechst-stained nuclei in each field were considered to represent total number of cells in each field. The following cell types were counted after staining; Cardiomyocytes (Sarc. MHC+, Cx40-), VCS cardiomyocytes (Sarc. MHC+, Cx40+), LDs storing cardiomyocytes (Sarc. MHC+, BODIPY+), LDs storing cells (BODIPY+), proliferating cardiomyocytes (Sarc. MHC+, Cx40-, Edu+), proliferating VCS cardiomyocytes (Sarc. MHC+, Cx40+, Edu+). Cell counts from each well were presented as percentages based on total number of nuclei counted in each well and analysed from a minimum of three independent experiments.

Embryonic heart cross-sections and immunohistochemistry

CD1 embryos from the E11.5 gestation stage were collected and placed in a cryoprotectant 30% sucrose solution overnight on a rocker at 4°C. The 30% sucrose solution was then discarded, and embryos were washed once with PBS. Embryos were then embedded in optimal cutting temperature embedding medium (O.C.T. compound, Thermo Fisher Scientific, Cat#4585) and cooled to -80°C to solidify and store. Thin, 10μM tissue sections were cut using Leica CM 3050 S microtome and collected on Superfrost® Plus slides (Thermo Fischer Scientific, Cat#12-550-15). Slides were stored at -20°C until further processing.

Slides processed for immunohistochemistry were taken out from -20°C to room temperature and air dried for 10 minutes. Sections were fixed using 4% paraformaldehyde for 15 minutes at room temperature and then permeabilization was done using 0.1% triton X 100 for 7 minutes. Sections were then blocked using blocking buffer solution (10% v/v goat serum, and 1% w/v bovine serum albumin in PBS) for one hour at room temperature. Primary antibodies diluted in blocking buffer were added to the sections and incubated overnight in 4°C humid chamber. Secondary goat anti-mouse antibody conjugated to Alexa Fluor 488 (or 555) (1:200, Thermo Fisher) and goat anti-rabbit antibody conjugated to Alexa Fluor 555 (or 488) (1:200, Thermo Fisher) were used. Nuclei were stained with 0.5μg/ml Hoechst 33258 in PBS for 3 minutes at room temperature. Finally, sections were incubated with BODIPY 493/503 dye at 1:1000 dilution (1μg/ml) for 20 minutes at room temperature, to stain lipid droplets in the cells. After washing with PBS, slides were mounted with 0.1% propyl gallate solution and a coverslip was put on. Immuno-stained sections were examined using a Leica DM2500 microscope and images were captured using a Leica DFC 500 digital acquisition system. To compare the different regions of the cross-section, the intensity of the target protein per unit area from 10 random fields was analyzed using ImageJ software.

In-cell westerns

In-cell westerns were performed for cells cultured in 96-well plates. Cells were fixed and permeabilized as described in the immunocytochemistry section. Incubation of primary antibodies was done as described for immune cytochemistry procedure. Anti-rabbit IgG (H+L) DyLight 800 PEG conjugate (New England Biolabs, Cat#515P), 1:150 dilution (6.67 μg/ml) and anti-mouse IgG (H+L) DyLight 680 conjugate (New England Bioloabs, Cat#5470P), 1:150 dilution (6.67 μg/ml) secondary antibodies were added for 1 hour at room temperature. Hoechst staining was performed as per the earlier-mentioned protocol. In-cell western images were captured and analyzed using the LI-COR Odyssey imaging system (Channels 700 and 800). The signal intensities of target proteins were normalized by Hoechst intensity (DNA content) acquired by POLARstar Omega microplate reader. In-cell western results were presented as fold change compared to the control group of the experiment.

Total RNA extraction and RT-qPCR

Total RNA was extracted from cultured embryonic ventricular cells using Aurum™ Total RNA Mini Kit (Biorad, Cat#732-6820) method described in protocol manual. The RNA content was quantified by using Implen NanoPhotometer. RNA samples with 260:280 absorbance ratio >1.8 were used for further gene expression experiments. Reverse transcription reaction was performed for RNA samples to convert into more stable cDNA using a SuperScript VILO kit (Thermo Fisher, Cat#18090010). The cDNA samples were stored at -20°C for real time quantitative PCR (RT-qPCR) gene expression analysis experiments. List of primer sequences used for RT-qPCR analysis are included in Table S1. The RT-qPCR reactions were performed using Biorad CFX Connect Real-Time PCR System. 40 amplification cycles (95°C for 15 sec and 60°C for 1 min) were followed by generation of melt curves (95°C, 60°C and 95°C, 15 sec each) to confirm the amplification of single primer product. For gene expression analysis of PPARα and PPARβ, TaqMan™ Fast Advanced Master Mix (Cat#4444557, Thermofisher Scientific) and TaqMan™ gene expression assays (Cat#4331182, Thermofisher Scientific) were used as reported earlier.[80] 3-6 independent RNA extracts from each group were used for RT-qPCR analysis. All the gene expressions were normalized with expression of GAPDH using ΔΔCT method and results were presented as fold change relative to the control groups.

Protein extraction and western blotting

For extraction of protein, embryonic ventricular cells were cultured in 35 mm dishes. After three days of incubation with drug treatments, cells were washed twice with cold PBS on ice platform. Further, 300μL of lysis buffer (1% NP40, 5mM EDTA, 150 mM NaCl and 50 mM Tris-HCl, pH 8.0 supplemented with 1X protease and phosphatase inhibitor, Thermo Scientific, Cat#1861281) was added to the dishes and cells were scrapped using cell scrapper. Scrapped cells in lysis buffer were collected in tubes and let sit on ice for 10 minutes. Scrapped cell suspension was sonicated using sonicator three times each 10 seconds with 10 seconds break on ice and left on ice for 15 minutes. The suspension was centrifuged for 15 minutes at 13000 rpm in 4°C, and supernatant was collected leaving cell pellet in the tube. Protein quantification was done using Bradford assay. Isolated protein was stored at -80°C for future use. The whole protein extract was separated by SDS-PAGE and transferred to nitrocellulose membrane. The membranes were incubated with 3% BSA blocking buffer for 1 hour. Membranes were immunoblotted using appropriate primary antibodies overnight at 4°C. Cx40 was used at 1:660 dilution (1.5μg/ml), HCN4 was used at 1:1000 dilution (1μg/ml) and GAPDH was used at 1:3000 dilution (0.3μg/ml). Then, Anti-rabbit IgG (H+L) DyLight 800 PEG conjugate, 1:3000 dilution and anti-mouse IgG (H+L) DyLight 680 conjugate, 1:3000 dilution secondary antibodies were used to visualize the protein expression in LI-COR Odyssey imaging system. Expression of proteins was analysed relative to the GAPDH protein on the membrane by densitometry using ImageJ software.

JC10 staining

JC-10 (AAT Bioquest, Cat#22204) solution was prepared as described by the manufacturer's protocol. 20μM JC-10 working solution was prepared and 100 μL of the working solution was spread over the unfixed E11.5 heart cross-section for 30 minutes in a dark chamber. Further, sections were washed with PBS twice and Hoechst nuclear staining was performed. Sections were examined using a 590nm filter in a Leica DM2500 microscope immediately after the staining and images were captured using a Leica DFC 500 digital acquisition system. JC-10 intensity was normalized with Hoechst intensity (DNA content) before the analysis.

Seahorse assay

Oxygen consumption rate (OCR) and Extracellular acidification rate (ECAR) were measured using XF24 extracellular flux analyzer (Seahorse Biosciences, North Billerica, MA, USA). Embryonic ventricular cells were prepared as described in the cell culture section. Cells were plated on 24-well Seahorse XF24 plates at 40,000 cells/well and cultured overnight before the treatment. OCR and ECAR measurements were done after treating cultures with or without ANP and A71915 for 24 hrs. For glucose oxidation analysis, the sensor cartridge was hydrated a day prior to the assay. On the day of assay, culture media was removed form culture and replaced with DMEM base medium (Agilent, Cat#103575-100) supplemented with 1 mM pyruvate, 2 mM glutamine, and 10 mM glucose. Cells were equilibrated at 37°C for 1 h before the measurements were taken.

For fatty acid oxidation assay, cell culture media was replaced by substrate limited medium comprising DMEM (Agilent, Cat#103575-100) with 0.5 mM glucose, 1 mM glutamine, 0.5 mM carnitine and 1% FBS 6 hours before the assay. Prior to assay, substrate limited medium was replaced by fatty acid oxidation buffer (Krebs Henseleit Buffer, 111 mM NaCl, 4.7 mM KCL, 2 mM MgSO4, 1.2 mM NaH2PO4, 1.25 mM CaCl2, 5 mM HEPES, 2.5 mM glucose and 0.5 mM carnitine) and cells were equilibrated for 1h at 37^{O}C. Sensor calibration was done as per

manufacturer's protocol before the assay. Assay was performed after adding BSA-oleic acid and BSA-linoleic acid cocktail (200μM each). A mitochondrial complex V inhibitor (oligomycin A; 1 μM, Focus Biomolecule, Cat#10-2092) was used to inhibit coupled respiration. An uncoupler of mitochondrial oxidative phosphorylation (Carbonyl cyanide-p-trifluoromethoxyphenylhydrazone; FCCP; 1 μM, MilliporeSigma, Cat#C2920) was used to analyze the uncoupled respiration. Finally, Rotenone (complex I inhibitor; 1 μM, MilliporeSigma, Cat#45656) and Antimycin A (complex III inhibitor; 5 μM, MilliporeSigma, Cat#A8674) were added to analyze the non-mitochondrial OCR. Assays were set up to record three measurements in each treatment and recorded OCR and ECAR were normalized to the total protein concentration in each well.

Lipid extraction and Ultra-HPLC method for lipid analysis

Lipid extraction was performed using the modified Bligh and Dyer extraction for LC-MS analysis of lipids protocol. All reagents used were of LC-MS grade. Cell pellets (~1 million cells) were obtained from embryonic ventricular cell cultures treated with or without ANP and or A71915 after 3 days of treatment. Cell pellet was homogenized in 1 ml of cold 0.1 M HCl:methanol (1:1, v/v) in a TissueLyser II instrument (Qiagen) set at 30 strokes/s for 2 to 4 min. Protein quantification was performed by BCA assay. Further, all samples were adjusted to the final concentration of 700 μg/ml and spiked with 10 μl of internal standard (Avanti Polar Lipids Inc; Catalog Number-330707). Each sample was added with 500 μl Chloroform, vortexed for 30 min, and centrifuged at 6000 rpm for 5 min to separate phases. The organic phase at the bottom was collected into a new Eppendorf tube and dried under a nitrogen stream. Samples were stored at −80°C until ready for analysis.

The Ultra-HPLC method was used for lipid analysis. The Accucore C30 column (250.2.1 mm I.D., particle size: 2.8 μm; Thermo Fisher Scientific) was used. The mobile phase system included solvent A and B of solvent A with 10 mM ammonium formate and 0.1% formic acid. Solvent A is acetonitrile:water (60:40 v/v) and solvent B is isopropanol:acetonitrile:water (90:10:1 v/v). C30-RPLC separation was performed at 30°C (column oven temperature) with a flow rate of 0.2 ml/min, and 10 μl of the lipid extraction suspended in the mobile phase solvents mixtures (A:B, 70:30) was injected onto the column. The lipid classes and molecular species were separated by following system gradient: 30% solvent B for 3 min followed by solvent B increased to 50% over 6 min, then to 70% B in 6 min, then at 99% B for 20 min. Finally, prior to each new injection, the column was re-equilibrated to starting conditions (30% solvent A) for 5 min.

High-resolution tandem mass spectrometry and lipidomics

Lipid analyses were done using a Q-Exactive Orbitrap mass spectrometer controlled by X-Calibur software 4.0 (Thermo Scientific) with an acquisition HPLC system. The parameters used for the Q-Exactive mass spectrometer were: sheath gas, 40; auxiliary gas, 5; ion spray voltage, 3.5 kV; capillary temperature, 250°C; mass range, 200 to 2000 m/z; full scan mode at a resolution of 70,000 m/z; top-1 m/z and collision energy of 35 (arbitrary unit); isolation window, 1 m/z; automatic gain control target, 1e5. The ESI negative and positive calibration solutions (Thermo Scientific) was used to calibrate the instrument to 1 ppm. Further, a mixture of lipid standards (Avanti Polar Lipids) was used optimized to tune parameters in both negative and positive ion modes. Lipid identification and quantitation was done by Thermo ScientificTM LipidSearchTM software version 4.2. Tandem mass spectrometry spectra of lipid precursor ions were searched in individual data files as described in a previous reports.[36,80] Fragment ions were predicted for all precursor adduct ions measured within ±5 ppm. The product ions that matched the predicted fragment ions within a ±5 ppm mass tolerance was used to calculate a match score, and those candidates providing the highest quality match were determined. Next, the search results from the individual positive or negative ion files from each sample group were aligned within a retention time window (±0.2 min) and the data were merged for each annotated lipid.

QUANTIFICATION AND STATISTICAL ANALYSIS

Data cleanup and statistical analysis of lipids

The LipidSearch software extracted the lipid concentrations and further analysis was done using an in-house script written in R programming language (version 4.0.2). The data were filtered and all the data with a signal-to-noise ratio (SNR) of smaller than 2 and a peak quality (PQ) of less than 0.8 was removed. Furthermore, if this filtration eliminated 2 of 3 replicates, the remaining replicate was also removed as untrustworthy. Following data filtration, replicate observations were averaged together and the normalized areas of all mass spectrometry fragments that correspond to a given lipid species were added together to generate the result. The results of obtained lipid groups containing multiple lipid concentrations corresponding to specific lipid identities were then compared between control and ANP and or A71915 treated samples using a (paired, nonparametric) Wilcoxon signed-rank test at an overall significance level of 5% (using the Bonferroni correction to account for the large number of tests performed). As the Bonferroni correction is conservative, significant differences are reported at both precorrection (*) and postcorrection (***) significance levels.

Statistical analysis

The statistical analyses for all other experiments were performed using GraphPad Prism software. All the data are presented as mean ± standard error of the mean (SEM). Two groups were compared using a two-tailed unpaired t-test. Multiple groups were analyzed using One- way ANOVA analysis and Dunnett's or Tukey's multiple comparisons tests. Correlation analysis was performed using Pearson correlation coefficient (r). $P<0.05$ were assigned as a significant result. The number of experiments and replicates is mentioned in the corresponding figure legends.